AD A106745

REPORT DOCUMENTATION PAGE		READ INSTRUCTIONS BEFORE COMPLETING FORM
1. REPORT NUMBER 79-258T	2. GOVT ACCESSION NO. AD-A106 745	3. RECIPIENT'S CATALOG NUMBER
4. TITLE (and Subtitle) Applications in Photoacoustic Spectroscopy.		5. TYPE OF REPORT & PERIOD COVERED THESIS/DISSERTATION
		6. PERFORMING ORG. REPORT NUMBER
7. AUTHOR(s) Robert Carl Ligday		8. CONTRACT OR GRANT NUMBER(s)
9. PERFORMING ORGANIZATION NAME AND ADDRESS AFIT STUDENT AT: The University of Texas at Austin		10. PROGRAM ELEMENT, PROJECT, TASK AREA & WORK UNIT NUMBERS
11. CONTROLLING OFFICE NAME AND ADDRESS AFIT/NR WPAFB OH 45433		12. REPORT DATE Aug 1979
		13. NUMBER OF PAGES 112
14. MONITORING AGENCY NAME & ADDRESS(if different from Controlling Office)		15. SECURITY CLASS. (of this report) UNCLASS
		15a. DECLASSIFICATION/DOWNGRADING SCHEDULE

16. DISTRIBUTION STATEMENT (of this Report)

APPROVED FOR PUBLIC RELEASE; DISTRIBUTION UNLIMITED

DTIC
ELECTE
NOV 6 1981
S
H
D

17. DISTRIBUTION STATEMENT (of the abstract entered in Block 20, if different from Report)

20 OCT 1981

18. SUPPLEMENTARY NOTES

APPROVED FOR PUBLIC RELEASE: IAW AFR 190-17

FREDRIC C. LYNCH, Major, USAF
Director of Public Affairs
Air Force Institute of Technology (ATC)
Wright-Patterson AFB, OH 45433

19. KEY WORDS (Continue on reverse side if necessary and identify by block number)

20. ABSTRACT (Continue on reverse side if necessary and identify by block number)

ATTACHED

81 10 26 146

DD FORM 1473 EDITION OF 1 NOV 68 IS OBSOLETE   UNCLASS

ABSTRACT

This thesis concentrates on three areas of photoacoustic (PA) spectroscopy: the correlation of experiment to solid state PA theory; electrochemical PA spectroscopy and the characterization of TiO_2 semiconductor materials with PA spectorscopy. Results are presented which show the relationship of the PA signal to the volume of the coupling gas, the dropping frequency and the sample concentration.

$\ddot{u}$

Accession For

NTIS GRA&I	
DTIC TAB	☐
Unannounced	☐
Justification	

By
Distribution/

Dist

A

APPLICATIONS IN PHOTOACOUSTIC SPECTROSCOPY

by

ROBERT CARL LIGDAY, B. S.

THESIS

Presented to the Faculty of the Graduate School of

The University of Texas at Austin

in Partial Fulfillment

of the Requirements

for the Degree of

MASTER OF ARTS

THE UNIVERSITY OF TEXAS AT AUSTIN

August 1979

Acknowledgements

The author wishes to express his appreciation
to Professor Allen J. Bard for his support and guidance
throughout this work.

The assistance and suggestions of fellow grad-
uate students Vic Fishman, Tim Henning and Cal Jaeger
proved invaluable.

The author recognizes the opportunity and finan-
cial assistance provided by the United States Air
Force Institute of Technology, Wright-Patterson Air
Force Base, Ohio.

<div align="center">R.C.L.</div>

Table of Contents

Chapter I. Introduction

Photoacoustic theory

The photoacoustic (PA) effect has seen a steady growth in applications during the past ten years. Applied since the 1930's to the study of relaxation phenomena in the gas phase [1,2], researchers today utilize PA spectroscopy to investigate the optical and thermal properties of solids [3,4] and solutions [5]. Reviews of the basic solid state theory and some of its original applications have been published [6-8].

Rosencwaig and Gersho [9,10] have developed and investigated the basic theory of solid state PA spectroscopy. The fundamental experiment is illustrated in Figure 1i. The sample, sealed in a gas tight cell of minimal volume, is irradiated with chopped monochromatic light. Energy absorbed by the sample and converted by non-radiative processes to thermal energy periodically heats a layer of gas adjacent to the sample. The temperature variations cause this layer to expand and contract at the chopping frequency creating a pressure wave which is transmitted through the gas volume and detected by a microphone. The PA signal observed is a function of the optical properties, the thermal properties and the physical dimensions of the

sample, the cell, and the coupling gas. Studies to date have been somewhat limited quantitatively because of difficulties in separating thermal from optical effects. The two principle advantages of PA spectroscopy are 1) the ability to obtain optical absorption spectra of totally opaque material and 2) the reduced contribution of scattered light effects.

Adams and Kirkbright, et.al., [11-16] published extensively results from PA experiments and experimental correlation to theory in systems involving ultraviolet, visible and near infrared irradiation of solids and solutions in both double and single beam instruments. Gray and Bard [17] reported the detection of gases evolved from photo-induced reactions. Rosencwaig, et. al., discussed applications in thin layer chromatography [18] and with biological materials [19]. Others have reported PA measurements for a variety of applications [20,21].

This work concentrates on three areas of PA spectroscopy: the correlation of experiment to solid state PA theory, electrochemical PA spectroscopy, a new technique; and the characterization of TiO_2 semiconductor materials with PA spectroscopy. Chapter two presents the results from a set of experiments which investigated the relationship of the PA signal to 1) the volume of the

coupling gas, 2) the chopping frequency, and 3) the sample concentration.

Rosencwaig and Gersho [9] have developed an expression for the complex envelope of the pressure variation (Q) for a solid sample in an ideal, cylindrical PA cell where the sample surface area, the perpendicular cross-section of the cell and the incident beam cross-sectional area are of the same dimensions.

$$Q = \frac{Y\beta}{k_s \alpha_g (\beta^2 - \sigma^2)} \tag{1}$$

$$X \left[\frac{(r-1)(b+1)\exp(\sigma_s \ell) - (r+1)(b-1)\exp(-\sigma_g \ell) + 2(b-r)\exp(-\beta \ell)}{(g+1)(b+1)\exp(\sigma_s \ell) - (g-1)(b-1)\exp(-\sigma_s \ell)} \right]$$

In Equation (1),

$$Y = \frac{\gamma P_o I_o}{2\sqrt{2}\, l_g T_o} \tag{2}$$

where γ is the ratio of specific heats (C_P/C_V), P_o and T_o are the ambient pressure and temperature, I_o is the incident light intensity, l_g is the length in centimeters of gas filled portion of the cell and

β = sample absorption coefficient, cm^{-1}

k_i = thermal conductivity of i, cal/cm sec °C

$a_i = (\omega/2\alpha_i)^{\frac{1}{2}}$

α_i = thermal diffusivity of i, cm^2/sec

ω = chopping frequency, rad/sec

$\sigma_i = (1 + j)a_j$ (complex value)

$r = (1 - j)\dfrac{\beta}{2a_s}$

$b = \dfrac{k_b a_b}{k_s a_s}$

$g = \dfrac{k_g a_g}{k_s a_s}$

ℓ = thickness of sample, cm

and s, g and b are subscripts corresponding to the sample, gas and backing material. From Equations (1) and (2) the resultant acoustic "plane" pressure wave varies as the inverse of l_g. Therefore, since the volume of a cylinder varies directly with the height, the pressure will vary inversely with the volume of the cell.

However, in many cell designs the incident light image is smaller than the sample surface area and the cross-section of the cell, i.e., a laser image. In these situations the resultant pressure wave is "spherical" and an additional r^{-1} dependence is imposed on its magnitude, where r is the radius of the sphere [22]. Assuming a low acoustic absorption at the walls of the cell, the pressure wave will propogate radially through the coupling gas to the microphone (Figure 1i). Since the volume (V) of a sphere (or section of sphere)

Figure 1. i) Schematic diagram of PA cell. a) sample,
b) coupling gas, c) window, d) cell wall,
e) incident light, f) thermally affected
gas layer, g) spherical acoustic wave.

ii) Optical absorption profile for sample
of thickness 1. $\mu_{s'}$ is less than μ_β.
$\mu_{s''}$ is greater than μ_β.

incident
light

μ_3

0 $\mu_{s'}$ $\mu_{s''}$ 1

sample thickness
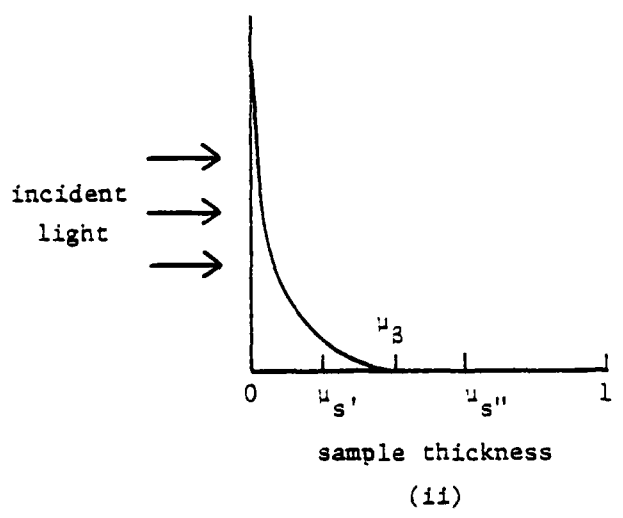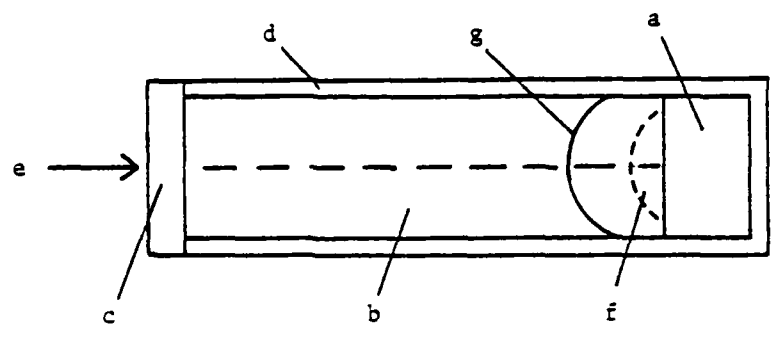
(ii)

varies as r^3, the pressure and the PA signal will vary as $V^{-1/3}$. It has been shown experimentally that this relationship holds for decreasing volumes until the cell dimensions approach the ideal cell.

In special cases Equation (1) can be simplified [9] and the dependence of the PA signal on chopping frequency determined. This has been experimentally shown for carbon black and a mixture of p-nitroanaline and silica gel. The relation of the optical absorption length, $\mu_\beta = 1/\beta$ to the thermal diffusion length, $\mu_s = 1/a_s$ is illustrated in an absorption profile, Figure 1ii. From the definition of a_s, μ_s varies as $\omega^{-\frac{1}{2}}$. For these optically opaque samples ($\mu_\beta << \ell$) when $\ell > \mu_s > \mu_\beta$,

$$Q \cong \frac{(1-j)}{2a_g}\left(\frac{\mu_s}{k_s}\right) Y \qquad (3)$$

the PA signal has a ω^{-1} dependence. However when $\mu_s < \mu_\beta$

$$Q \cong \frac{-j\beta\mu_s}{2a_g}\left(\frac{\mu_s}{k_s}\right) Y \qquad (4)$$

and the PA signal is proportional to $\omega^{-3/2}$, as only the energy absorbed within the thermal diffusion layer will contribute to the PA signal.

The relationship of PA signal to concentration

of absorbing species in solid mixtures was investigated

for possible application to thin layer chromatography.

Mixtures of absorbing samples with a low absorbing

diluant at various concentrations were studied.

The absorption coefficients for some materials

were found to be sufficiently large that a "saturation"

effect was observed. In this situation, for optically

opaque samples when $\mu_s > \mu_\beta$ the PA signal is β indepen-

dent, Equation (3), and becomes only dependent on the

power of the incident light. When normalized to that

power spectrum, the sample spectrum loses its optical

character. Diluting the sample with a low absorbing

material such as silica gel effectively reduces the

absorbtion of the mixture, resulting in an increased μ_β.

When dilution is sufficient that $\mu_\beta > \mu_s$, the PA signal

becomes β dependent, Equation 4.

Chapter III describes an application of PA

techniques to electrochemical systems. A simple

electrochemical-PA (ECPA) cell was designed, fabricated,

and tested. The complex theory involving such a

technique will not be discussed here. However, the

basic principle is illustrated in a block diagram

(Figure 2). Thermal energy emitted from an optically

absorbing material deposited on the working electrode

9

Figure 2.   Schematic diagram of electrochemical-PA cell.

electrochemical
cell

electrode

microphone

incident
light →

→

window

sample
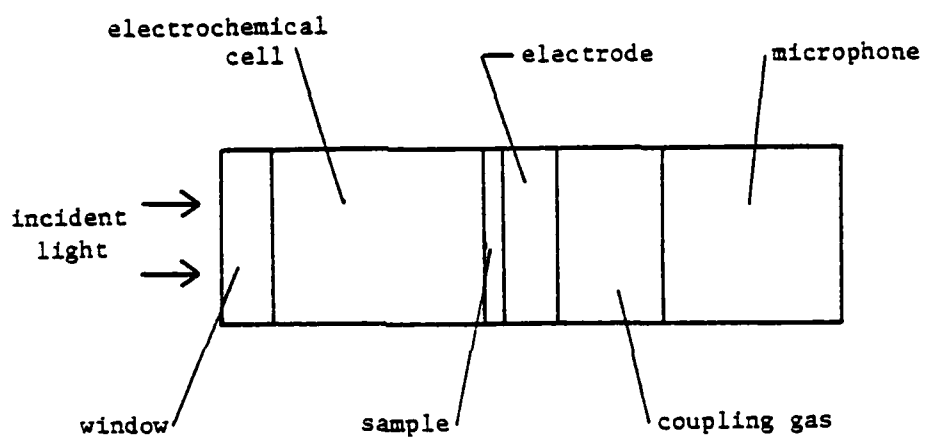
coupling gas

in an electrochemical cell, radiates in part through
the sample to the electrode. The electrode, possessing
a high thermal conductivity, transmits the thermal
energy to the coupling gas. And, as in conventional
PA techniques, a pressure wave is detected by a micro-
phone.

The feasibility of this technique was tested
with the colored film heptyl-viologen radical cation
(from 1,1-diheptyl-4,4-bipyridinium di bromide) in
a prototype three electrode cell. After improvements
in the cell design, thin films of tungsten oxide
(WO_3) were anodically generated from a tungsten elec-
trode. Extensive investigations of the viologen films
[23,24] and the WO_3 films [25-27] have been reported
for their use in electrochromic displays. PA spectra
were recorded for these films and a PA detection limit
based upon the WO_3 film thickness was determined.

The characterization by PA spectroscopy of
titanium dioxide (TiO_2) powders and rutile crystals
is discussed in Chapter IV. Anatase powders treated
in N_2 at temperatures above 600°C were converted to
the rutile structure as confirmed by x-ray diffraction.
The rutile (powder and crystals) and the anatase
(powder) TiO_2 were reduced in hydrogen and vacuum,
respectively, by heating at temperatures lower than

600°C to TiO_{2-x}, where x increases with duration of heating [28]. PA spectra of the various samples were recorded and the changes in signal magnitude and spectral character are discussed.

PA Spectrometer

The essential components of our single beam PA spectrometer are depicted schematically in Figure 3. The light source, a 2500 watt, high pressure, xenon, compact arc lamp, provided an effective spectral range of 300-800 nm when coupled with a grating monochromator. The collimated beam was focused with a single lens onto the entrance slit of the monochromator. Light exiting the monochromator fit with 10 nm slits was focused onto the sample as a rectangular image of approximately 0.36 cm^2 area. Slits of 2 and 6 nm, were used to enhance resolution, when higher signals premitted. Cut off filters of 50% transmition at 390 and 630 nm were utilized to filter higher order reflections from the grating (blazed at 6000 Å). A mechanical chopper provided a frequency range of 5 to 1800 Hz through the use of interchangeable blades with 2, 6, 19 and 60 slots. The upper frequency limit was a result of acoustic vibrations from the high speed chopper blade which constructively interfered with acoustic detection in the cell. To minimize these effects, the

Figure 3. Block diagram of PA spectrometer.
a) light energy source, 2.5 K watt Xenon
lamp, b) chopper, c) monochromator, d) PA
cell, e) lock-in amplifier, f) data acquisi-
tion and storage.
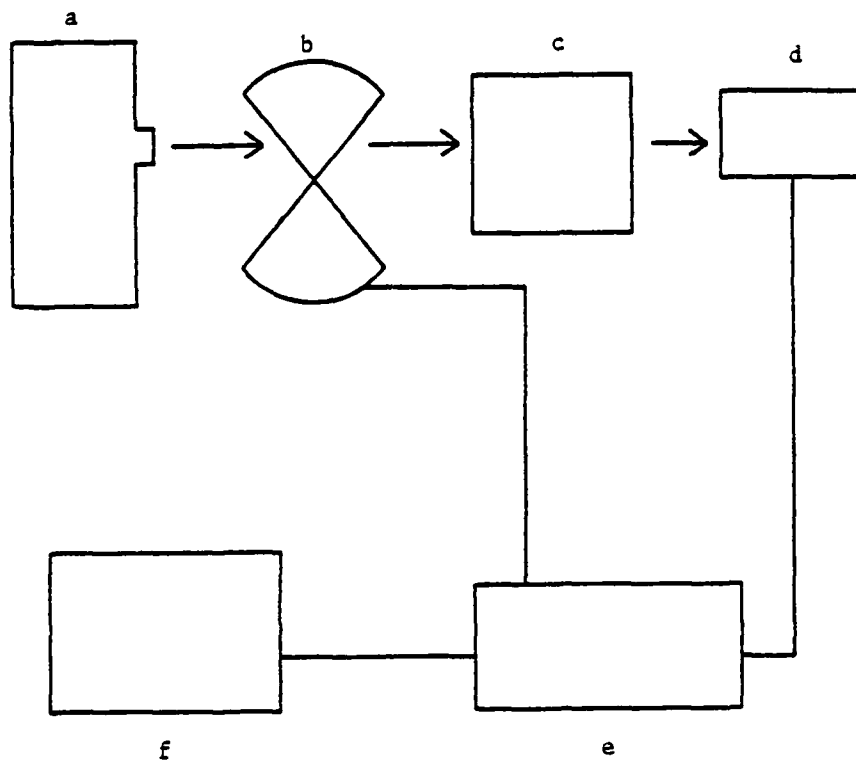
chopper blade was placed as far from the cell as possible.

Three different PA cells were used in these studies; a simple quartz cuvet cell, an aluminum body cell, and an electrochemical-PA (ECPA) cell. A one inch General Radio ceramic microphone was used in each cell. The random incidence response curves were flat over 20 to 2000 Hz.

The simply designed quartz cell (Figure 4) was fabricated with a sawed off quartz cuvet with a volume of 2.22 cm^3 serving as the body of the cell. Samples were placed into the cell through the top before positioning of the microphone. A metal face plate with a 7 mm diameter hole was attached with silicone adhesive (Dow-Corning) to the microphone providing a smooth surface on which to temporarily seal the cell with silicone grease (Dow-Corning). The principle disadvantage of this cell, was the inability to consistently mount solid samples. The method used was to fix the sample to a glass plate with double-faced sticky tape.

The aluminum body cell was milled from a single cylinder of 60-61 grade aluminum and fitted with a quartz window (Figure 5). Air-tight seals were made with O- rings around the microphone and at the base of
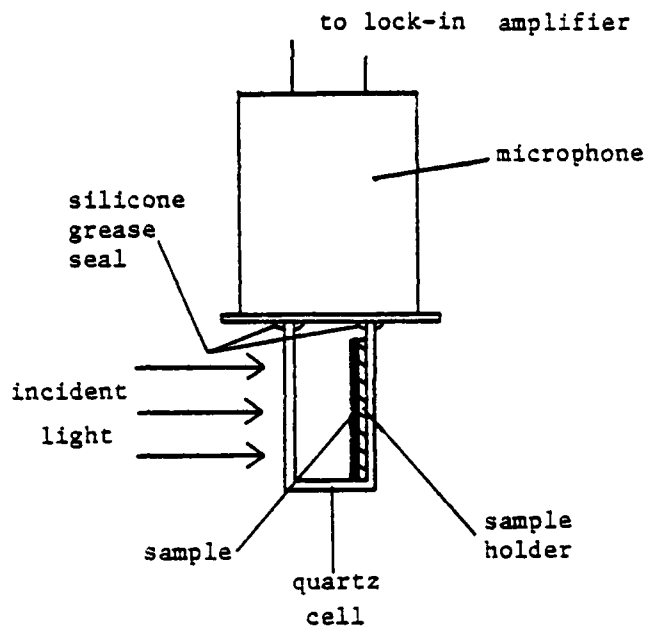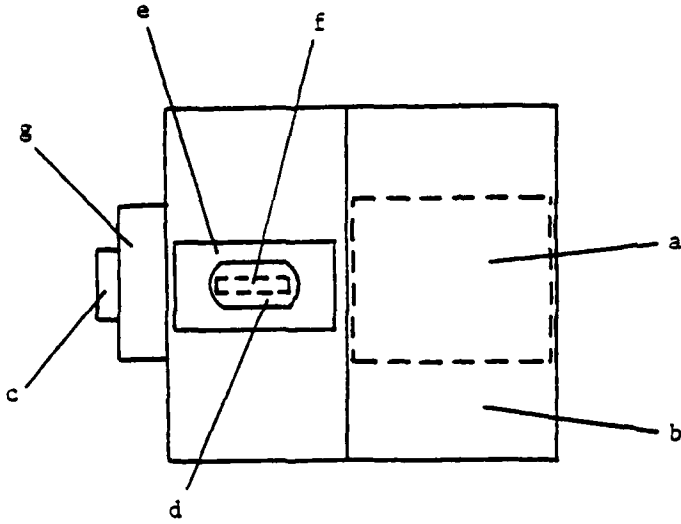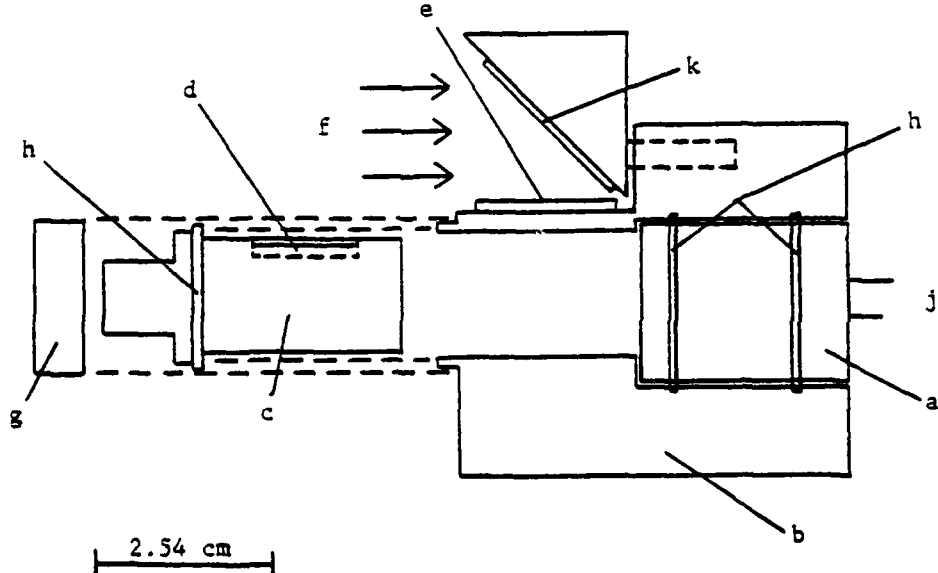
Figure 4.   Quartz PA cell

to lock-in amplifier

microphone

silicone
grease
seal

incident

light

sample

quartz
cell

sample
holder

2.54 cm

18

Figure 5.   Aluminum body PA cell (i) and top view (ii).
             a) microphone, b) aluminum body, c) sample
             holder, d) sample, e) quartz window, f) inci-
             dent light, g) threaded ring, h) O-ring
             seals, j) to lock-in amplifier, k) first
             surface mirror.

(ii)

2.54 cm

(i)

two interchangeable aluminum sample holders. The boat-like design of the sample holders afforded minimal sample preparation. A specified amount of sample deposited into the holder and spread evenly on the flat bottom was ready for placement into the cell. The disadvantage of using this cell with certain samples was the low level absorption of the aluminum, which sometimes provided a relatively high background signal. The background was observed with transparent samples such as single crystal titanium dioxide and with highly reflective metals such as copper or platinum foil. The ECPA cell will be discussed in Chapter III.

The PA cell was isolated from the optical bench by mounting it on a platform supported by an inner tube (16 in. OD) through which mechanical noise transmitted from instrumentation was damped.

The dual output voltages of the microphone were fed directly to a lock-in amplifier placed in the differential input mode and referenced to the chopping frequency. The lock-in was equipped with a 0.1 sec dc pre-filter and 5 and 50 Hz high band pass and 100 and 10K Hz low band pass frequency filters. Signals were generally processed with 0.3 sec time constant at a maximum monochromator scan rate of 1.67 nm/sec. The effective detection range of the lock-in was 1 μV

to 250 mV, although the PA signal never exceeded 1 mV.

Signals processed from the lock-in were input to either a two-channel data storage scan recorder or a multichannel data processing recorder. A lamp power spectrum obtained with a carbon black (bone charcoal) sample was used for normalization and is shown in Figure 6. Normalized PA spectra were recorded on paper for permanent record. The component instrumentation of the PA spectrometer are listed by function in Table I with manufacturer and model numbers.

Figure 6. Power spectrum of Xenon lamp taken with carbon black sample in the aluminum body cell. Arrows indicate change of cut off filters.
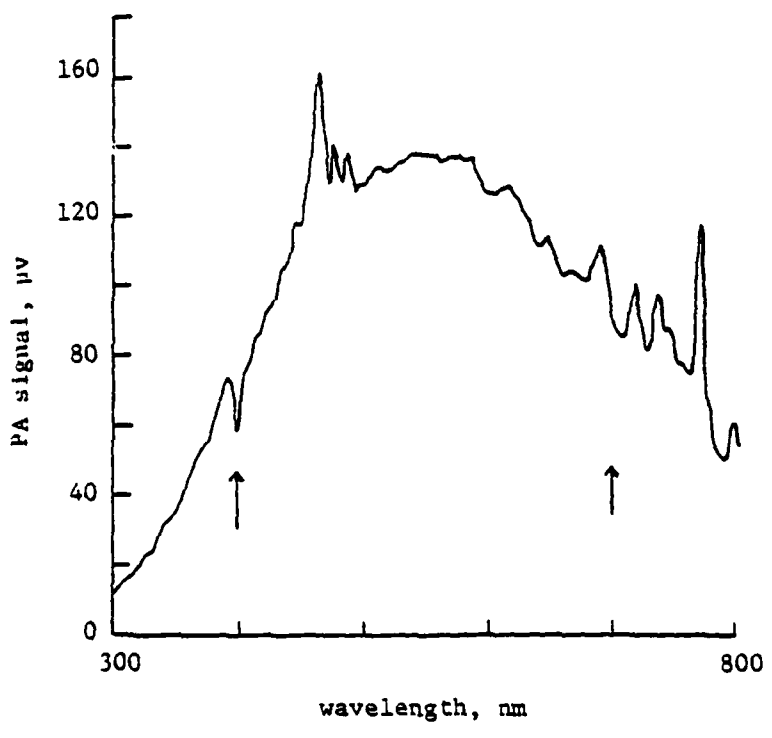
wavelength, nm

TABLE I: COMPONENT INSTRUMENTATION OF

PHOTOACOUSTIC SPECTROMETER

	FUNCTION	MANUFACTURER	DESCRIPTION AND MODEL
1.	Lamp	Canrad-Hanovia	High pressure xenon compact arc lamp, 975CO390
2.	Lamp Housing	Schoeffel Instrument Co.	Universal lamp housing, Model LH152N
3.	Lamp Power Supply	Hanovia, Inc.	Compact arc lamp power supply, Model 28151
4.	Starter	Hanovia, Inc.	200 amp starter, Cat. No. 29912
5.	Chopper	Princeton Applied Research	Variable frequency light chopper, Model 192
6.	Monochromator	Jarrel-Ash $f/4$ Model 82560	1/4 Monochromator
7.	Microphone	General Radio Co.	Microphone, Model 1560-9065
8.	Lock-in	Princeton Applied Research	Lock-in analyzer, Model 5204
9.	Recorder	Princeton Applied Research	Scan recorder, Model 4101
10.	Recorder	Bascom-Turner Instruments	Electronic recorder, Model 8110

Chapter II. Correlation of Experiment to Solid State

PA Theory
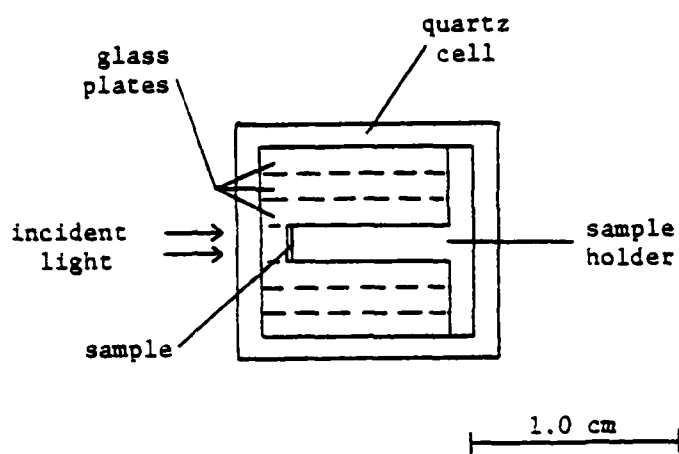
Volume of coupling gas vs. PA signal

The dependence of the PA signal of the coupling
gas (air) volume was studied for volumes less than 2 cm^3.
The quartz cell with a special "T" shaped sample holder
was used (Figure 7). Six interchangeable glass plates
cut from microscope slides fit into the quartz cell
and served to vary the volume between 0.27 and 1.61 cm^3.
A carbon black powder sample was fixed on the holder
with double faced tape and its position relative to
the microphone was constant throughout the experiment.
Volume measurements were calculated from the total
volume of the cell minus the measured volume of the
plates. Plates were considered a uniform volume, 0.22
cm^3 ± 2% as verified by weighing. The total volume
of the cell with sample in place was 1.61 cm^3. PA sig-
nals were measured in microvolts at 453 and 540 nm.

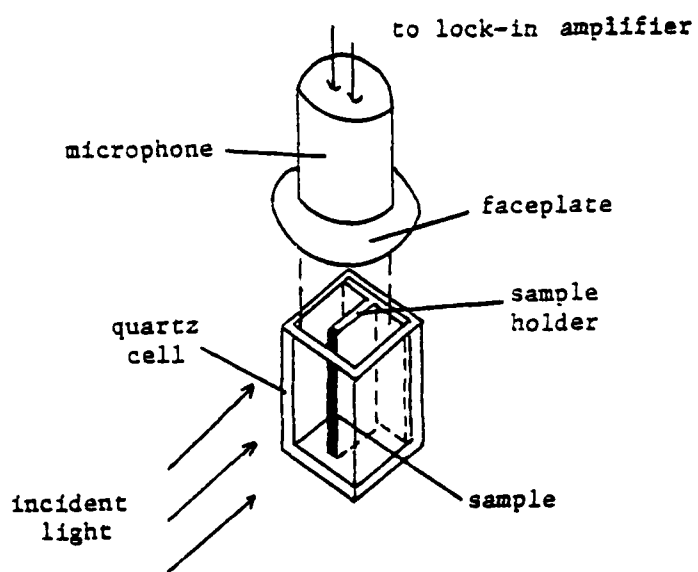The PA signal is plotted versus volume (V) in
Figure 8i. As predicted the signal increases as the
volume of the coupling gas decreases. A plot of PA
signal versus $V^{-1/3}$ (Figure 8ii) shows linear depen-
dence and indicates a spherical wave form. At smaller
volumes deviation from the linear least squares regres-
sion calculated from the first six points suggest a

Figure 7.   Quartz cell and sample holder (i) used for volume of coupling gas experiment and top view (ii).   Six glass plates were used to vary the volume from 1.61 to 0.27 cm^3.
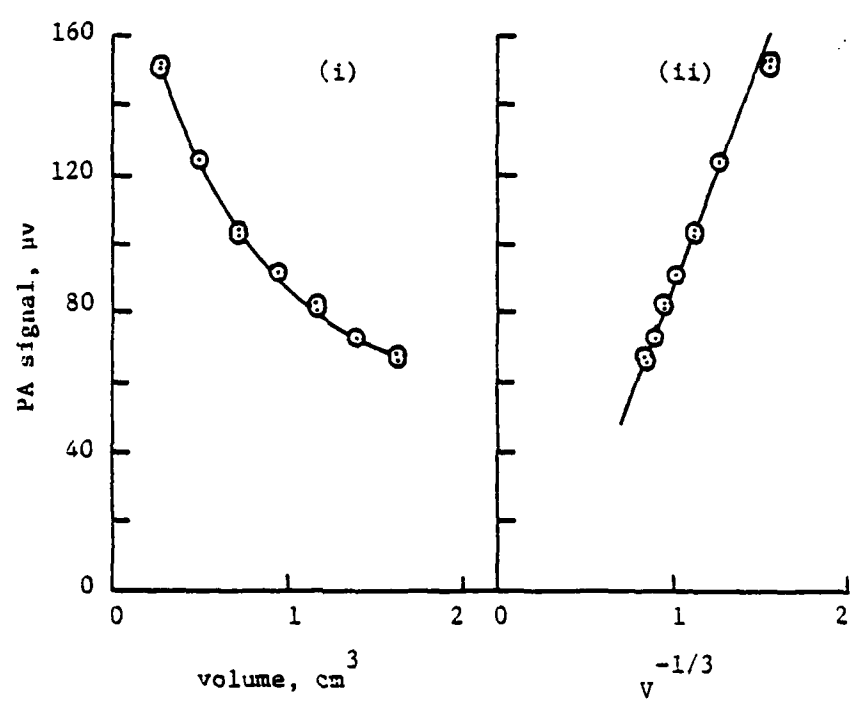
glass plates

quartz cell

incident light

sample holder

sample

1.0 cm

(ii)

to lock-in amplifier

microphone

faceplate

quartz cell

sample holder

incident light

sample

(i)

Figure 8. Volume of coupling gas dependence of PA
signal for carbon black sample. i) PA
signal versus volume. ii) PA signal versus
the reciprocal of the cubed root of the
volume.

loss of spherical wave character. The walls closing in
on the sample would reduce the spherical pressure wave
form to one resembling a plane wave. Thus the relation-
ships of the geometries of the cell, to the incident
light image and the sample are important to considera-
tions in cell design for a maximum PA signal. Cells
in which these parameters are not closely matched
allow for an unnecessary loss of signal.

Chopping frequency vs. PA signal

The PA signal as a function of chopping fre-
quency was determined for a carbon black sample
using the aluminum cell. PA signals were measured
over 15 Hz to 550 Hz at 5 Hz intervals through 250 Hz
and then 50 Hz intervals to 550 Hz, and are plotted
versus the frequency (radians/second) in Figure 9i.
The logarithmn of the PA signal versus the logarithmn
of the frequency (Figure 9ii) shows an $\omega^{-1.03}$ fre-
quency dependence which is well within experimental
error of the predicted ω^{-1} for solid samples with
$\mu_\beta << \ell$ and $\mu_s > \mu_\beta$.

A similar experiment was conducted with a mix-
ture of p-nitroaniline diluted to 0.188 µg/mg of
silica gel (Mallinckrodt TLC-7). Figure 10, the
logarithm of the PA signal versus the logarithm of
the frequency (rad/sec), shows a change in frequency

31

Figure 9. Frequency (ω) dependence of PA signal for
carbon black sample. i) PA signal versus
frequency. ii) Logarithm of PA signal ver-
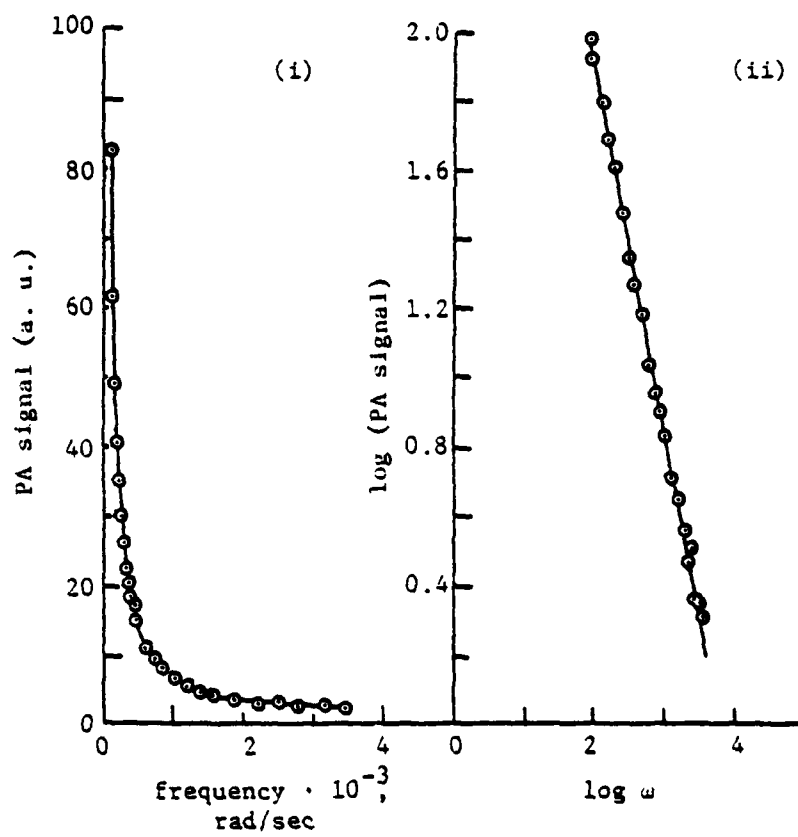sus logarithm of frequency, slope is -1.03.

Figure 10. Frequency (ω) dependence of PA signal for a sample mixture of p-nitroaniline and silica gel, 1.88×10^{-4} p-nitroaniline by weight. On the logarithm of PA signal versus logarithm frequency plot, the slope changes from -0.98 (a) to -1.47 (b) based on least squares regression of first three and last three data points. The intersection of (a) and (b) is 2.75, or 89 Hz.
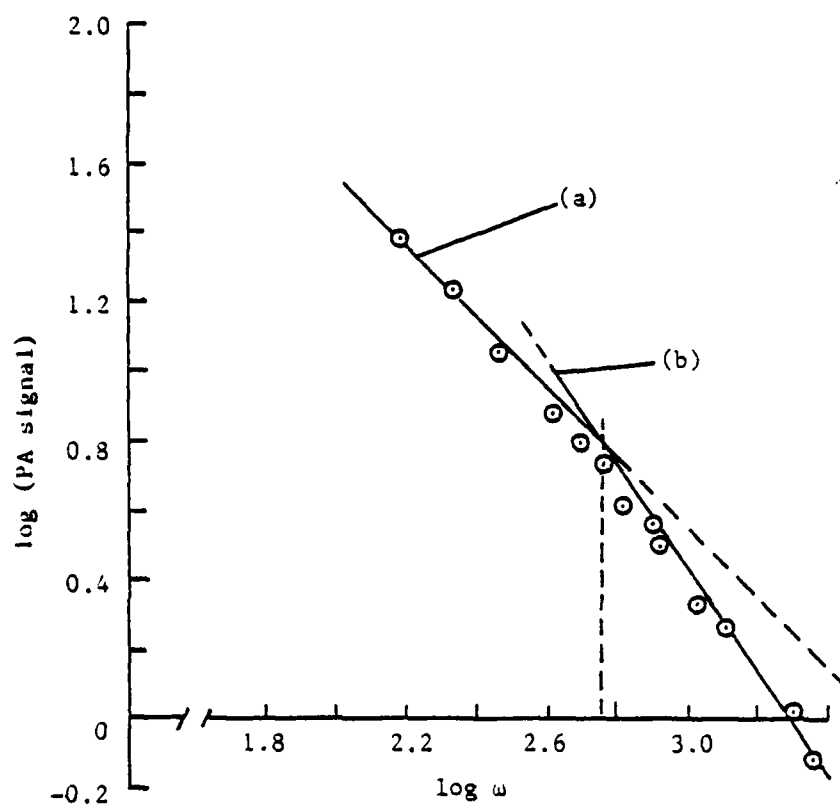
dependence. Slopes of the linear least squares regressions calculated from the first three and the last three experimental points are -0.98 and -1.47 respectively, indicating a switch in the relative magnitudes of μ_s and μ_β. The intersection of the two extrapolated lines determined that $\mu_s = \mu_\beta$ at 560 rad/sec (89 Hz). With this information; and either the thermal diffusivity of the mixture or the absorption coefficient, the other can be calculated. Although data such as this is not significant for the mixture studied, it demonstrates experimentally the application of the technique.

Concentration vs. PA signal

Mixtures of highly colored compounds and low absorbing powders were studied with PA spectroscopy in the aluminum cell. Rose bengal powder, 4,5,6,7-tetrachloro-2',4',5',7'-tetraiodofluorescein, (Eastman Kodak Co.) a common red dye, was mixed with magnesium oxide, MgO, (Fischer Scientific Co.) a fine white powder with a low PA response. Eight mixtures ranged in concentration from 2.1% to 49.4% rose bengal by weight. Pure rose bengal exhibited PA saturation at wavelengths shorter than 600 nm. Resolution of this effect was not observed with any of these mixtures. The PA signal at 540 nm normalized to the pure rose

bengal was determined to vary linearly with concentrations between 2.1% and 35% (Figure 11).

The same experiment was accomplished with mixtures of p-nitroaniline, a yellow dye, and silica gel (TLC-7) with concentratins ranging from 7.16×10^{-3}% to 1.16% p-nitroaniline by weight. Samples were prepared by applying measured volumes of a 1.66×10^{-2} $\underline{M}$ solution of p-nitroaniline in ethanol to weighed amounts of silica gel and allowing the solvent 24 hours to evaporate.

Normalized PA spectra from 580 to 300 nm for the seven concentrations are reproduced in Figure 12. The broken line represents a Cary 14 absorption spectra for a 1×10^{-4} $\underline{M}$ p-nitroaniline in ethanol solution. The PA saturation effect observed in the pure dye was resolved at all concentrations. The agreement between the absorption band centered at 384 nm obtained by PA spectroscopy of the diluted samples and the solution spectroscopy was excellent. The PA signal at the absorption peak normalized to pure p-nitroaniline is plotted versus concentration in Figure 13. A linear portion of the curve was determined, but found to deviate at concentrations lower than 5×10^{-3}% by weight. This deviation is probably a result of the difference in the thermal parameters of p-nitroaniline

Figure 11. PA signal correlation to concentration of
sample mixtures of rose bengal and magnesium
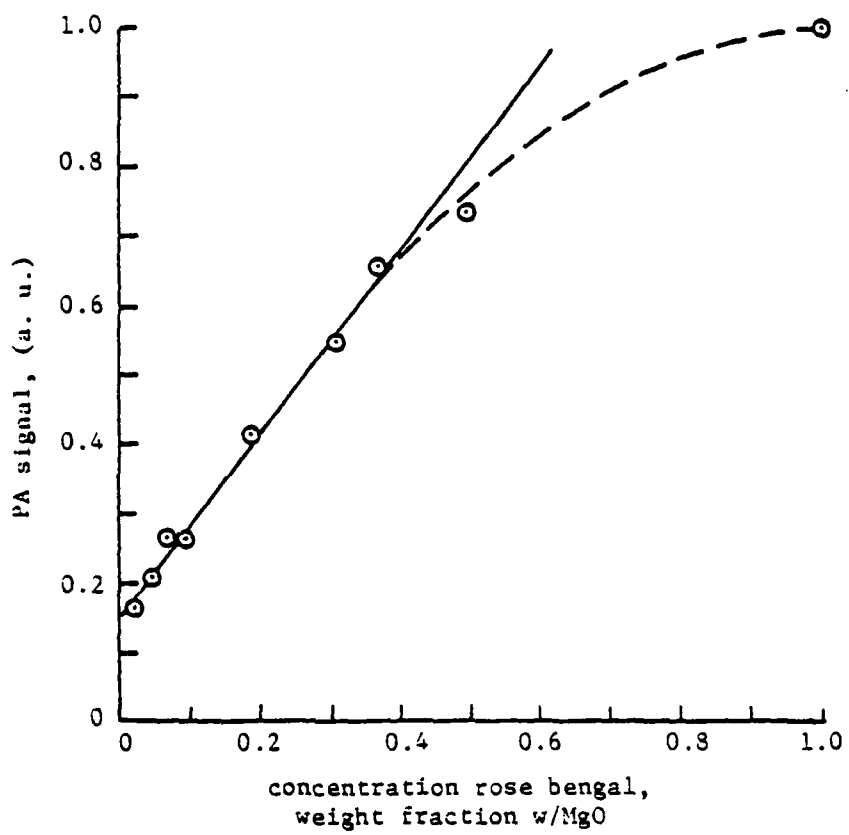oxide. PA signals are normalized to pure
rose bengal signal.

concentration rose bengal,
weight fraction w/MgO

Figure 12. Normalized PA spectra of p-nitroaniline mix-
            tures with silica gel, demonstrating resolu-
            tion from saturation effect. The broken
            line represents a solution absorption spec-
            trum of 1.0×10^{-4} M solution of p-nitro-
            aniline in ethanol. Concentrations of
            solid mixtures in weight fraction; a) 1.00,
            b) 1.2×10^{-2}, c) 5.8×10^{-3}, d) 4.8×10^{-4},
            e) 3.3×10^{-4}, f) 2.4×10^{-4}, g) 1.9×10^{-4},
            h) 7.2×10^{-5}.

normalized PA signal, (a. u.)
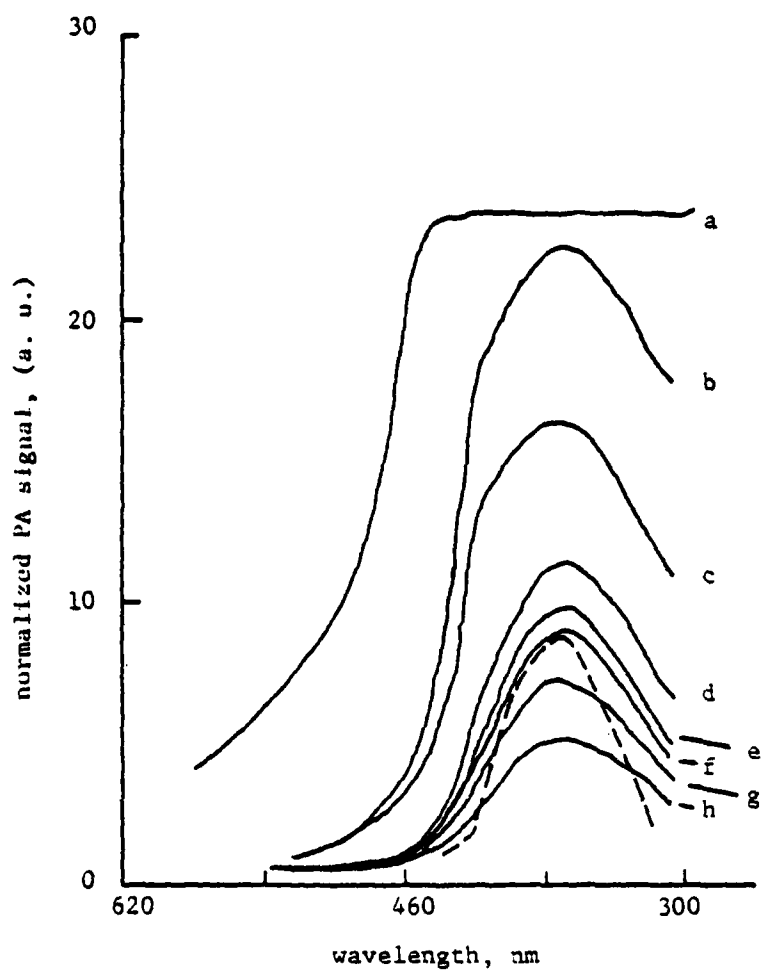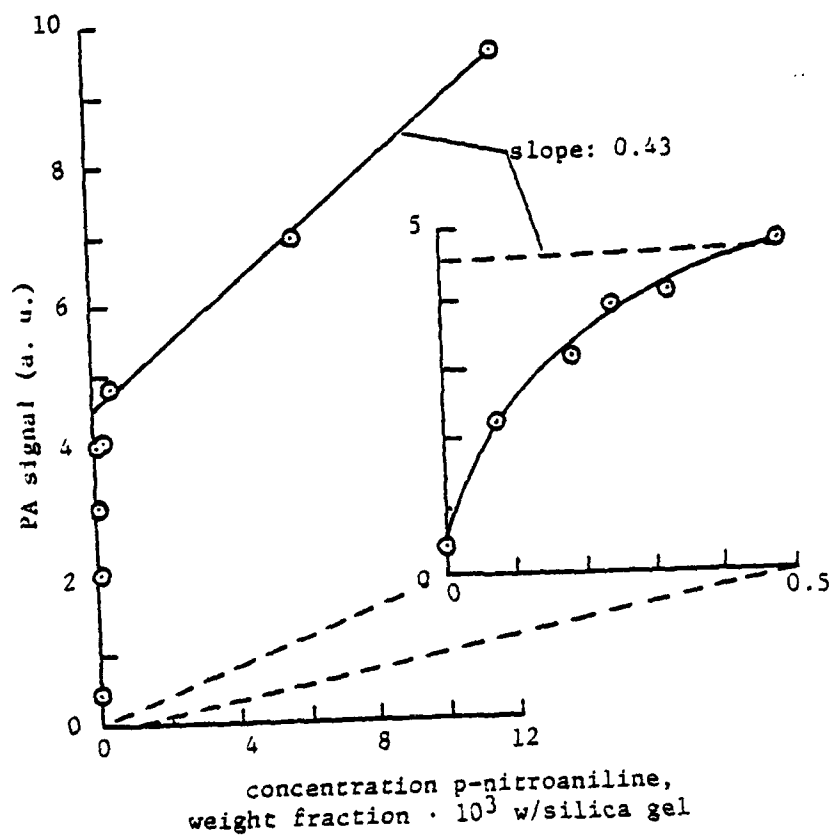
wavelength, nm

Figure 13. PA signal correlation to concentration of

sample mixtures of p-nitroaniline and

silica gel. PA signals correspond to 384 nm.

The inset expands the concentration scale

by a factor of ten.

concentration p-nitroaniline,
weight fraction · 10^3 w/silica gel

and silica gel, and the change of thermal parameters of the mixture over the range of concentrations.

The application of PA techniques in thin layer chromatography (TLC) can be demonstrated. From Touchstone [29], in TLC, a 1 cm^2 spot produced on a 250 μm thick layer of silica gel from a 1-5 μl sample of a 1-5 μg/μm solution of p-nitroaniline will result in concentrations from 2 x 10^{-3}% to 50 x 10^{-3}% by weight, within the range studied here. Thus PA techniques can be used to identify and to determine typical concentrations of highly absorbing materials studied in TLC from the silica gel/sample mixtures eliminating additional sample preparation.

Chapter III. Photoacoustic Detection of Thin Films

The PA effect was coupled with electrochemical techniques in the study of two systems, the reduction of heptyl viologen dication and the formation and reduction of tungsten oxide (WO_3), each of which formed highly colored thin films at an electrode surface in solution.

The ECPA cell

The application of the PA effect to detecting thin flims electrochemically generated on metal electrodes was tested using the electrochemical-PA (ECPA) cell diagrammed in Figure 14i. The working electrode, metal foil sandwiched between two glass plates, separated the solution from the coupling gas. Films generated on the solution side of the working electrode were exposed to chopped monochromatic light. The resulting thermal energy radiated in part through the sample and the metal electrode to the coupling gas were the ensuing pressure pulse was detected by the microphone.

The working electrode (6.5 x 24.5 x 0.025 mm), shown in Figure 14ii, was fastened with epoxy cement (Devcon Corp. 5 Minute Epoxy) between two glass plates (25 x 30 x 1.2 mm) centered over matching rectangular holes (5 x 17 mm). A narrow frame of epoxy cement was

Figure 14. Electrochemical-PA cell (i) and blow-up
of working electrode holder (ii). a) metal
foil working electrode, b) copper wire,
c) quartz window, d) counter electrode,
e) reference electrode, f) microphone, g) to
lock-in amplifier, h) glass cell, j) stand,
k) electrode surface exposed to incident
light, l) glass plates, m) silver paint and
epoxy cement, n) epoxy cement frame.
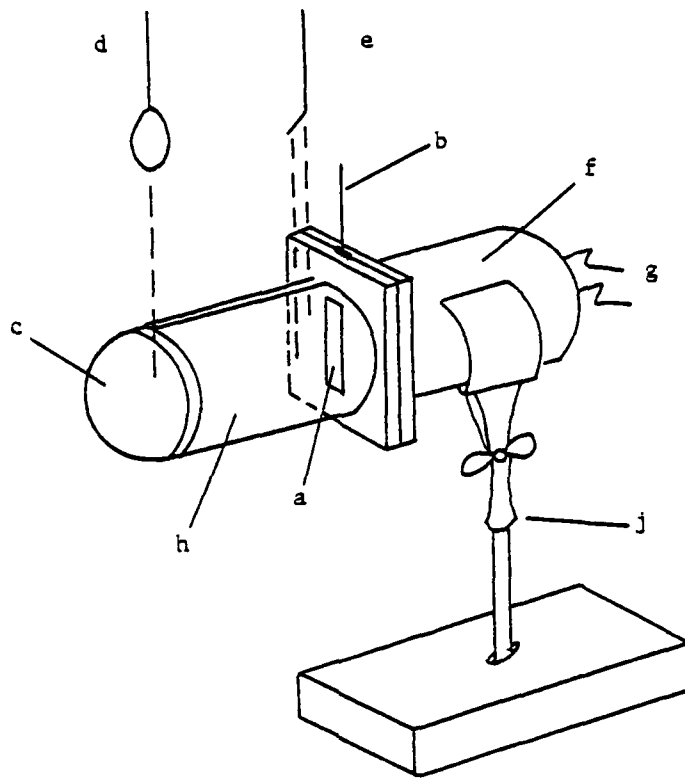
(i)
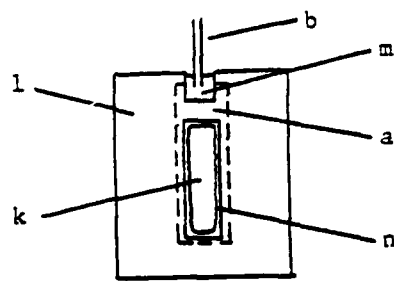
(ii)

placed in the corner between the metal and the glass on both sides of the electrode to assure an air tight/-solution tight seal. The working area of the electrode, 0.56 cm^2, was slightly larger than the area of the incident light image, 0.36 cm^2 for 10 nm band pass slits. Electrical contact was made at the top of the electrode with a copper wire and conducting silver paint held in place with epoxy cement. This electrode sandwich was fixed to both the solution cell and the microphone grill with silicon adhesive (Dow-Corning), a flexible adhesive providing air tight seals while affording easy disassembly for electrode replacement. (In the initial ECPA experiments with heptyl viologen the working electrode was not fixed, but loosely positioned in a slot between the glass plates and sealed with vacuum grease. The new design reduced the noise level in the PA signal significantly.)

The body of the cell was constructed from a 2.6 cm section of glass tubing (21 mm ID) with a quartz window (25 mm diameter) fixed to one end, with epoxy cement. The counter and reference electrodes were supported without contacting the cell body through a 1.5 mm slit, to minimize vibrations transmitted through the connections from the electrochemical measurement instrumentation.

Electrochemical measurements were made with a potentio-
stat, Princeton Applied Research, Corporation (PAR)
Model 175, and a digital coulometer, PAR Model 179.
Current-potential curves were recorded on a Houston
Instruments, Inc. Model 2000 X-Y recorder.

Heptyl viologen

The heptyl viologen radical cation (I)

$$R-\overset{+}{N} \bigcirc\hspace{-0.3em}\bigcirc N\cdot-R$$

$$R = C_7H_{15}$$
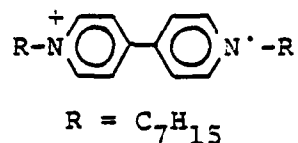
I

was formed at a platinum electrode in a reversible one
electron reduction from the di-cation in a 9.53 c 10^{-3}
$\underline{M}$ diheptylbypyridinium dibromide solution. The support-
ing electrolyte was 0.294 $\underline{M}$ potassium bromide. A
silver wire positioned near the working electrode
served as a quasi reference. A rectangular platinum
foil counter electrode with a surface area of 1.0 cm^2
was placed opposite the working electrode out of the
beam of incident light. The platinum electrode sur-
faces were cleaned in nitric acid and rinsed with
distilled water before each experiment. The silver
wire was scraped with fine sandpaper and rinsed with
distilled water. Solutions were prepared with distilled
water.

The PA absorption spectrum of the platinum electrode open to air and in solution are shown in Figure 15. The characteristic increasing absorption at shorter wavelengths was similar to that observed by Brilmeyer and Bard with photothermal spectroscopy [30]. The reduction in signal magnitude of more than 50% with the addition of the solution was found to occur with any liquid. This was probably due to the difference in thermal parameters of the solution and air, resulting in a relative heat sink effect of the solution, and to the damping of physical motion of the membrane electrode.

In a blank solution of 0.3 $\underline{M}$ KBr a small current representative of an irreversible reduction was measured negative of -0.2 v vs. Ag. This was probably the reduction of oxygen in the open cell. The presence of oxygen played a major role in the instability of the radical cation film, which rapidly oxidized to the soluble dication at open circuit. Attempts to seal the cell or de-aerate with a nitrogen flow resulted in unacceptable noise levels in the PA signal.

The typical cyclic voltamagram of the reversible one-electron reduction of heptyl viologen is shown in Figure 16. The half-wave potential was measured at -0.327 V vs. Ag. The shape of the cathodic

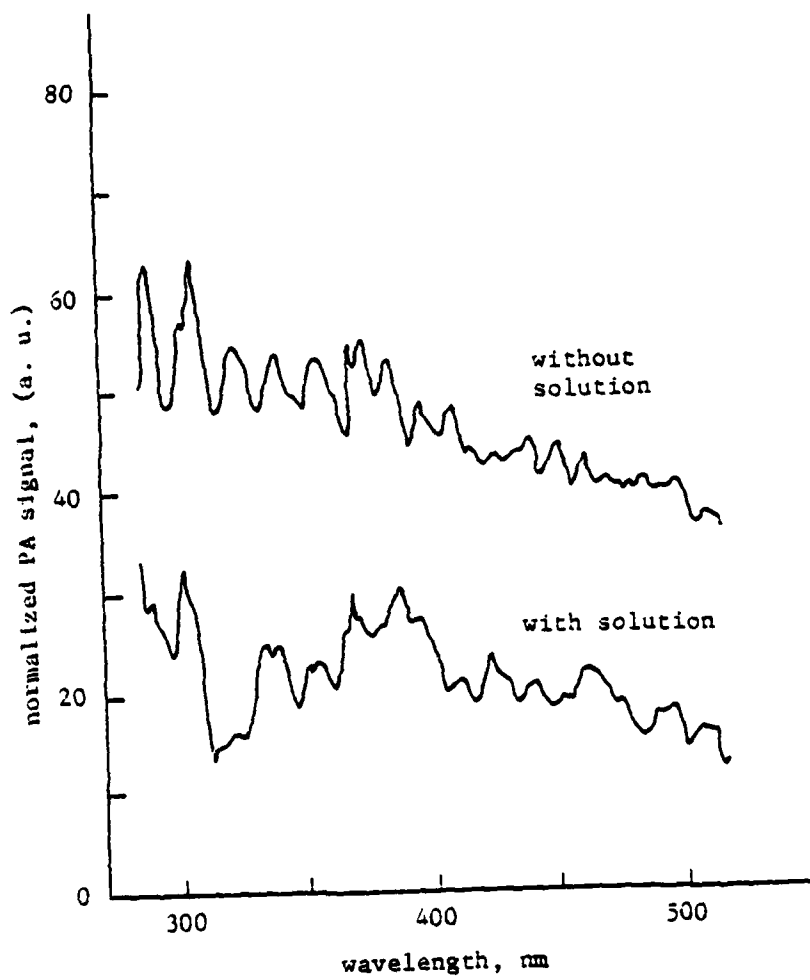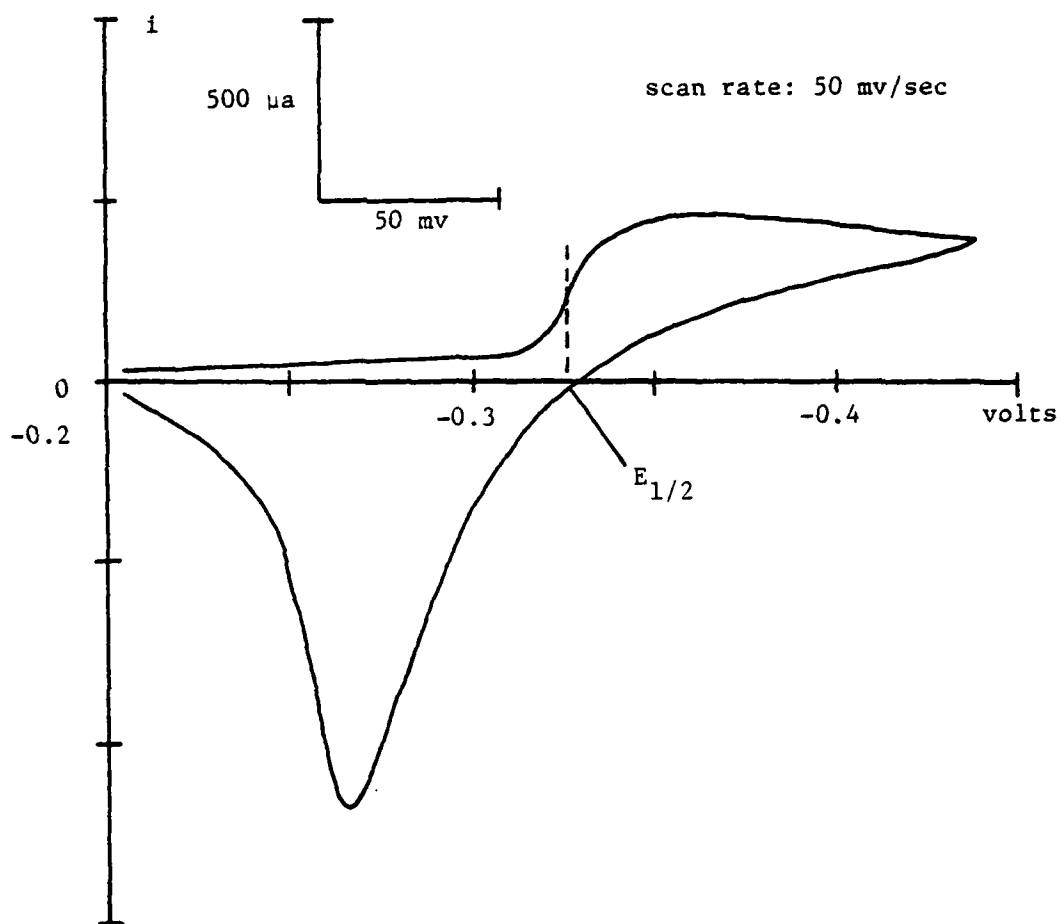Figure 15. Normalized spectra of platinum working
electrode.

52

Figure 16.   Cyclic voltamagram of heptyl viologen system.
$E_{1/2}$ is -0.327 volts vs Ag.

wave does not resemble that of a one-electron diffusion controlled reduction as expected in this system. The deviation to higher current at more negative potentials is probably due to the instability of the film. The cation radical oxidized by air to the dication at the electrode surface would be available for a repeated reduction (kinetically controlled).

The heptyl viologen was detected with the PA effect during the potential scan when cycling between 0.07 V and -0.47 V vs. Ag periodically deposited and stripped off the film. Figure 17 shows the PA response to 463 nm light (10 nm bandpass slits) as a function of time during several cycles at various scan rates. Also included is the PA response with no light during a cycle. The absence of a PA signal confirmed its dependence on the photo-absorption of the film, not on heating due to current flow.

The PA signal (PAS) is related to the amount of heptyl viologen deposited on the electrode by

$$PAS \stackrel{\sim}{=} \int idt \qquad (3)$$

where the current (i) for a diffusion controlled process is

$$i = Av^{\frac{1}{2}} \qquad (4)$$

In Equation (4), A is a constant dependent upon the initial concentration of the dication, its diffusion

55

Figure 17. PA response to deposit and stripping of
heptyl viologen film on a platinum elec-
trode at several scan rates. Arrows up
indicate beginning of deposit. Arrows
down indicate stripping.
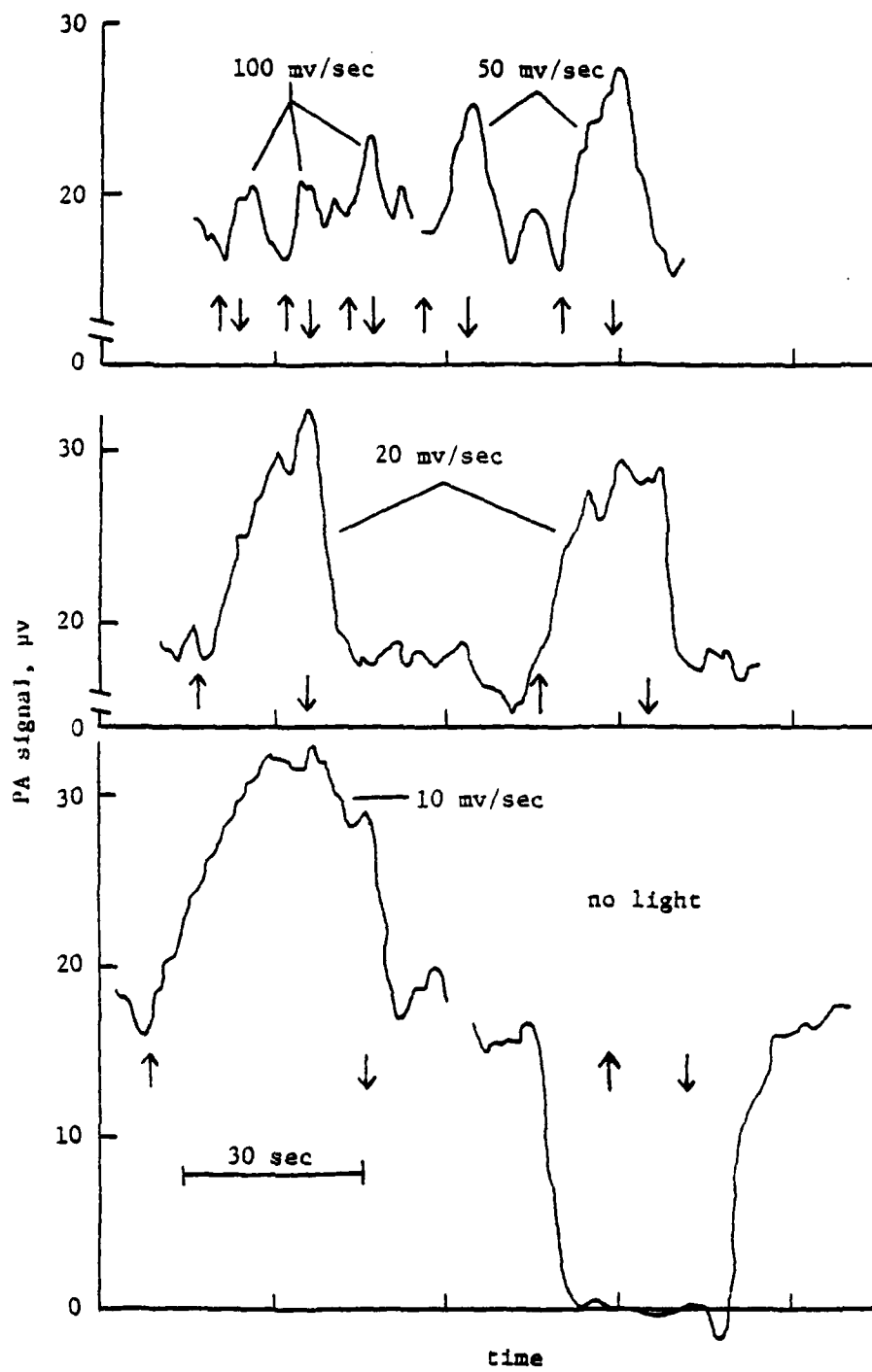
coefficient and the electrode surface area, and
v is the scan rate in volts per second.

$$v = \Delta E / t \tag{5}$$

From Equation (5)

$$t = \Delta E / v \tag{6}$$

and

$$dt = -\tfrac{1}{2}\Delta E v^{-2} dv \tag{7}$$

Substituting Equations (4) and (7) into Equation (3)
and carrying out the integration,

$$PAS = (const) v^{-\tfrac{1}{2}} \tag{8}$$

Thus for a diffusion controlled process, the PA signal
will have a inverse square root dependence on the scan
rate. The PA signal (measured above background) is
plotted versus scan rate in Figure 18i. The $v^{-\tfrac{1}{2}}$
dependence, in Figure 18ii, shows the deviations from
a diffusion controlled process, most evident at slower
scan rates.

The instability of the radical cation in this
system hindered attempts to obtain absorption spectra
of a thin film. The spectra shown in Figure 19 was
obtained by pulsing the potential between 0.01 v and
-0.47 v vs. Ag at one second per pulse (2 second
period). The effects of the double modulation from
1) the periodic deposition and stripping at 0.5 Hz
and 2) the chopped light at 30 Hz are evident in the

Figure 18.   i) PA signal dependence on scan rate for
             heptyl viologen system.   ii) PA signal
             versus the reciprocal of the square root of
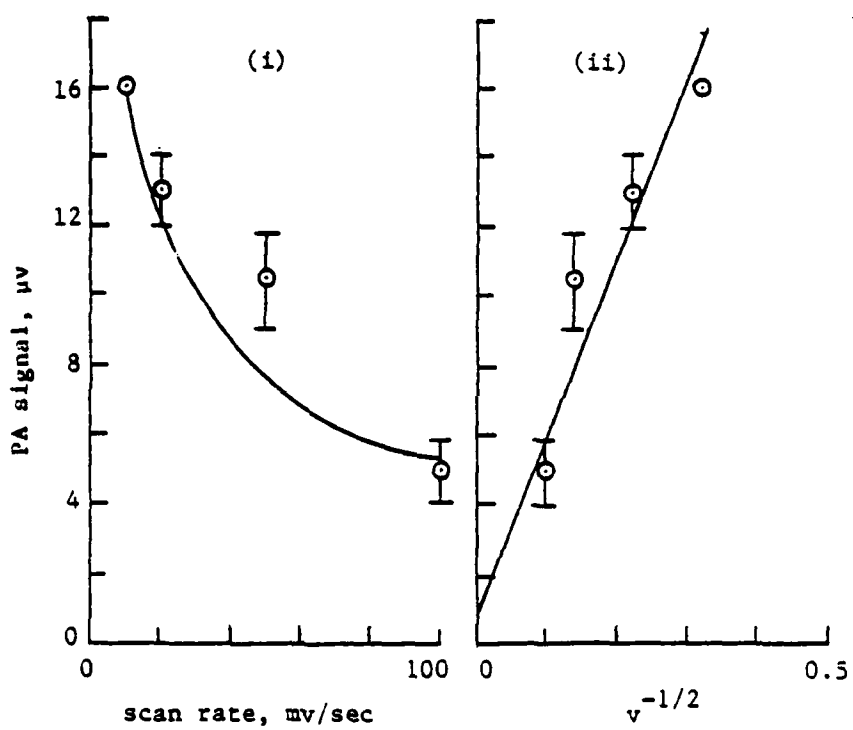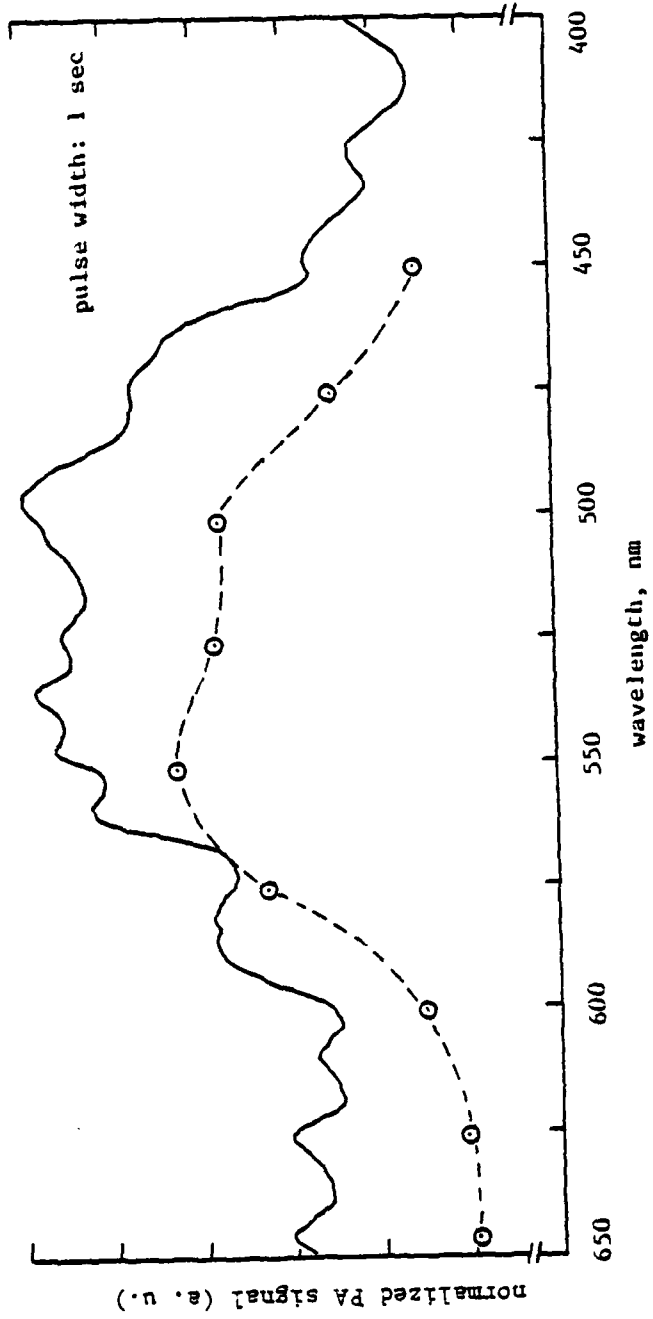   scan rate.

60

Figure 19. Normalized PA spectrum of heptyl viologen
film pulse deposited at a platinum
electrode. Broken line represents
absorption spectrum of heptyl viologen
thin film on tin oxide substrate (ref. 23).

pulse width: 1 sec

normalized PA signal (a. u.)

wavelength, nm

wavy character of the spectrum. Faster pulse deposition rates produced too little viologen to be detected, while slower rates resulted in noisier, non-descript spectra. Attempts to lock-on to the pulse deposition frequency with an unmodulated light source failed as pulse rates slow enough to produce detectable amounts of the film were too slow to be analyzed by the lock-in amplifier.
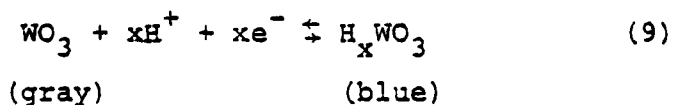
Tungsten Oxide

In the EPCA cell, stable films of tungsten oxide (WO_3) were anodically grown from a tungsten electrode and absorption spectra were recorded. The tungsten was oxidized in a 1.0 $\underline{M}$ sulfuric acid solution using a WO_3 coated tungsten wire quasi-reference and a platinum wire counter electrode. The reference electrode, was prepared by applying a potential between a 0.5 mm diameter tungsten wire and a platinum counter electrode in a 1 $\underline{M}$ H_2SO_4 solution. The potential was gradually increased to 65 volts at currents less than 25 milliamps. This procedure produced a WO_3 film approximately 1 μm thick. The counter electrode was a platinum wire, shaped into a ring to allow passage of the incident light while maintaining reasonable current distribution to the working electrode. Its total surface area was 0.80 cm^2.

A copper wire lead was attached to each electrode
with conducting silver paint and epoxy. The platinum
electrode was cleaned in nitric acid and rinsed
with distilled water before each experiment, while
the WO_3 coated and tungsten electrodes were only rinsed
in distilled water.

A PA spectrum of the tungsten electrode was
recorded before growth of a WO_3 film. Typical
spectra with and without the sulfuric acid solution
are shown in Figure 20. The reduction in signal
with the addition of solution was similar to that
observed with a platinum electrode.

A thin WO_3 film can be grown by cycling the
voltage between 1.0 v and -0.67 v vs. WO_3/W. A
typical cyclic voltamagram is shown in Figure 21.
The irreversible oxidation wave at potential greater
than 0.8 v represents the formation of WO_3 at the
surface of the tungsten electrode. The redox wave
at negative potentials represents the reversible
formation of H_xWO_3, where x is less than 0.5. The
color

$$WO_3 + xH^+ + xe^- \rightleftarrows H_xWO_3 \qquad (9)$$
$$\text{(gray)} \qquad\qquad \text{(blue)}$$

change of interest for electrochromic displays is
associated with this reduction.

Figure 20.   Normalized PA spectra of Tungsten working
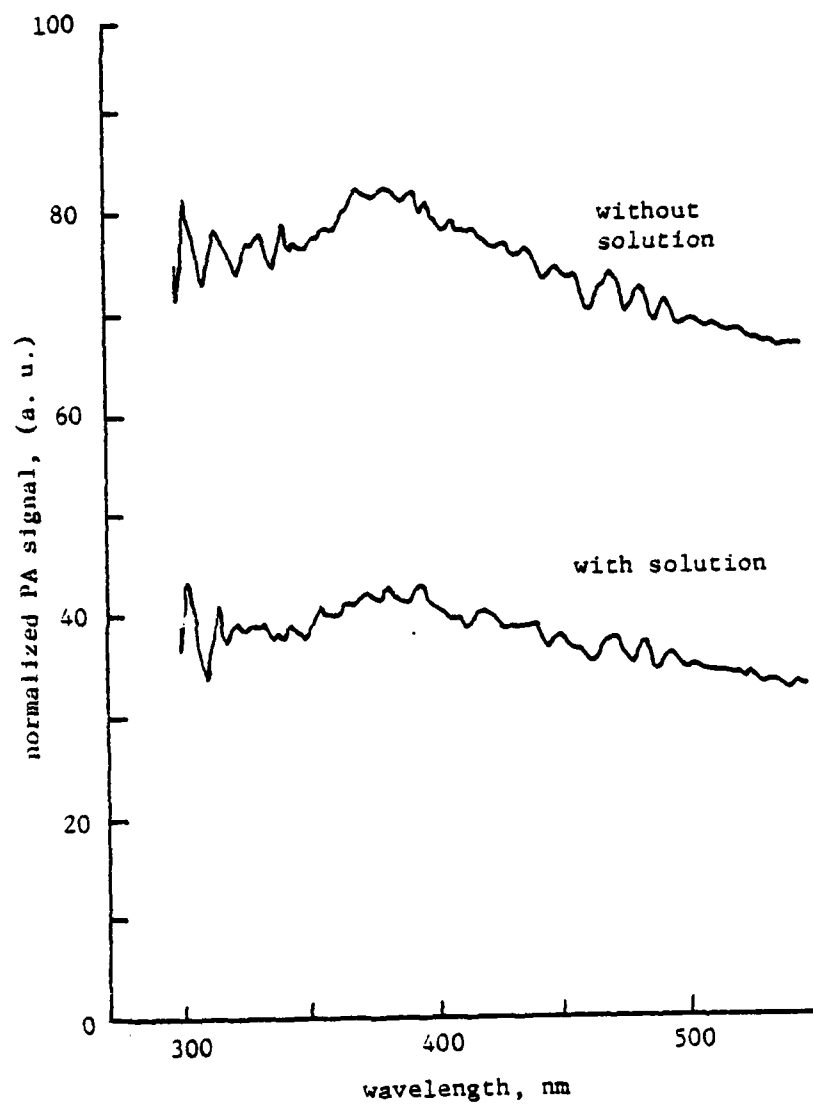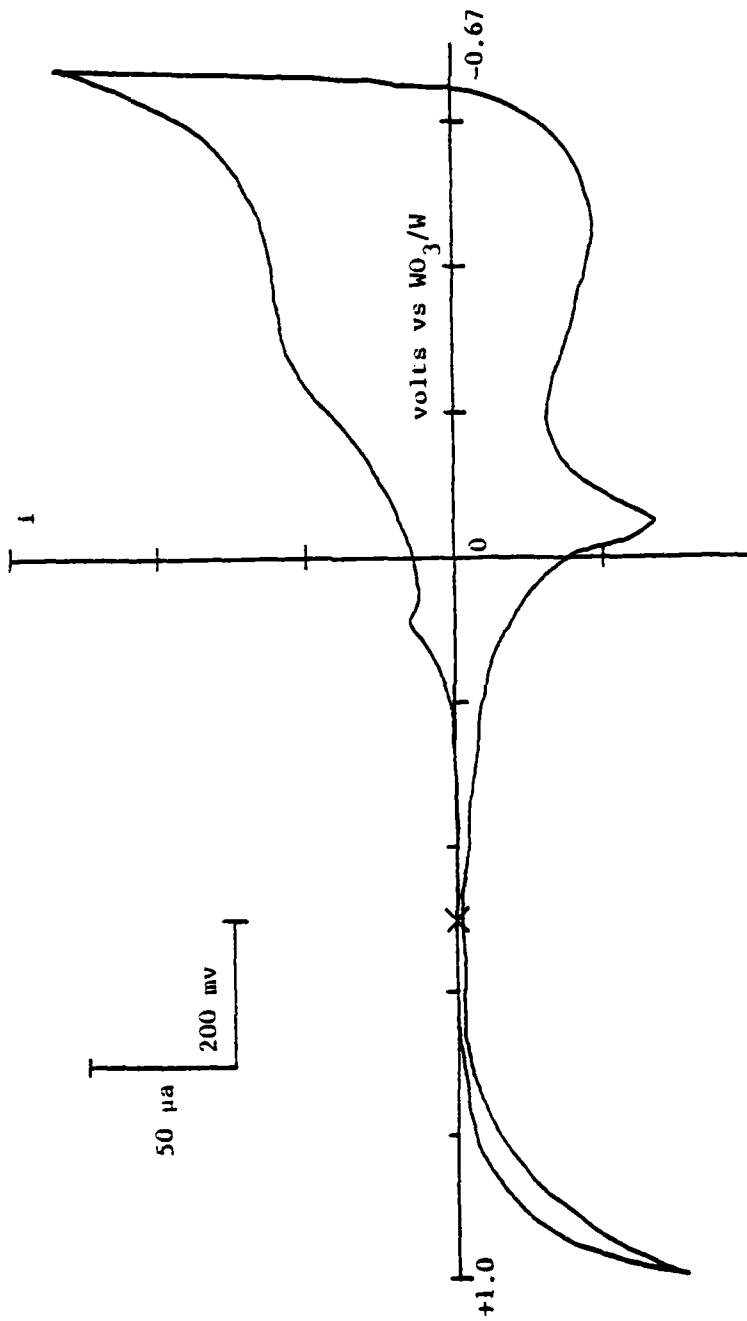
electrode.

66

Figure 21. Cyclic voltamagram of tungsten oxide system. Oxidation wave at positive potentials is growth of WO_3 from tungsten. Reversible wave at negative potentials is reduction of WO_3 to H_xWO_3.

The thin film was first observed while cycling through the coloration process. Figure 22 shows the PA signal using 550 nm light at 30 Hz of two cycles plotted against time. The peaks represent the blue reduced film. The PA signal as a function of potential was recorded for several cycles, one of which has been blown up and is shown in Figure 23. The interesting observation is the lag in the PA response to the bleaching of the film. The bleaching process was reported by Reichman [27] to take place in 10 msec. Therefore, the lag in the PA response of 0.6 sec is probably related to the thermal diffusion rate through the sample and the electrode. With fast processes such as this, the ECPA technique could be used to determine thermal diffusivities of electrode materials by varying their thickness and observing the corresponding change in lag time.

PA spectra of the band edge region for both the WO_3 and the reduced films were obtained by holding the potential at 0.45 and -0.60 v respectively before placing the cell at open circuit. Typical spectra of each, normalized to the lamp power, are shown in Figure 24. The absorption at the longer wavelengths of the reduced (blue) film is similar to that reported by Deb [25] from transmission spectra

Figure 22. PA response to potential sweep in WO_3 system.
Blue is color of reduced H_xWO_3 and gray is
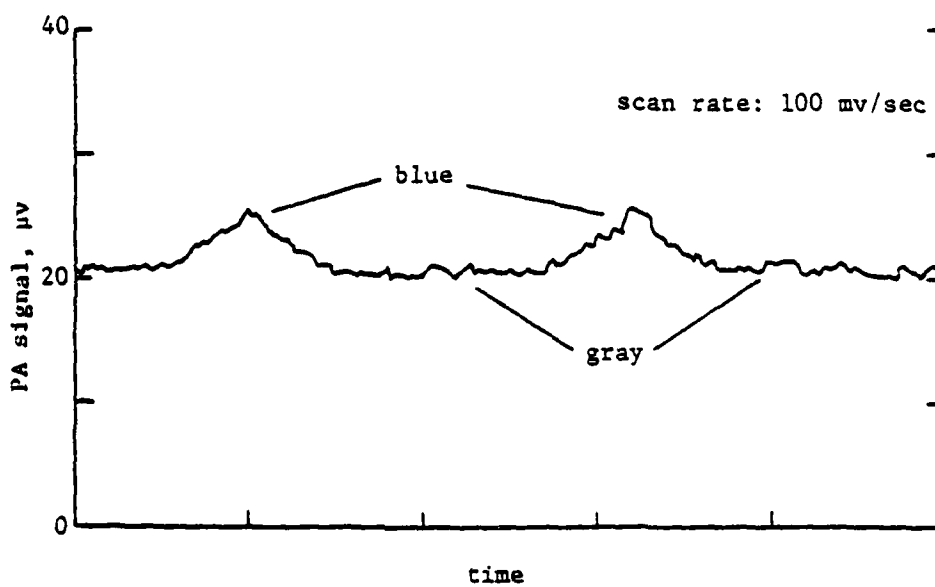color of WO_3 film.

scan rate: 100 mv/sec

Figure 23.   PA signal versus potential for one sweep

cycle in WO_3 system.   There is a 0.6 sec

lag in the PA response.

73

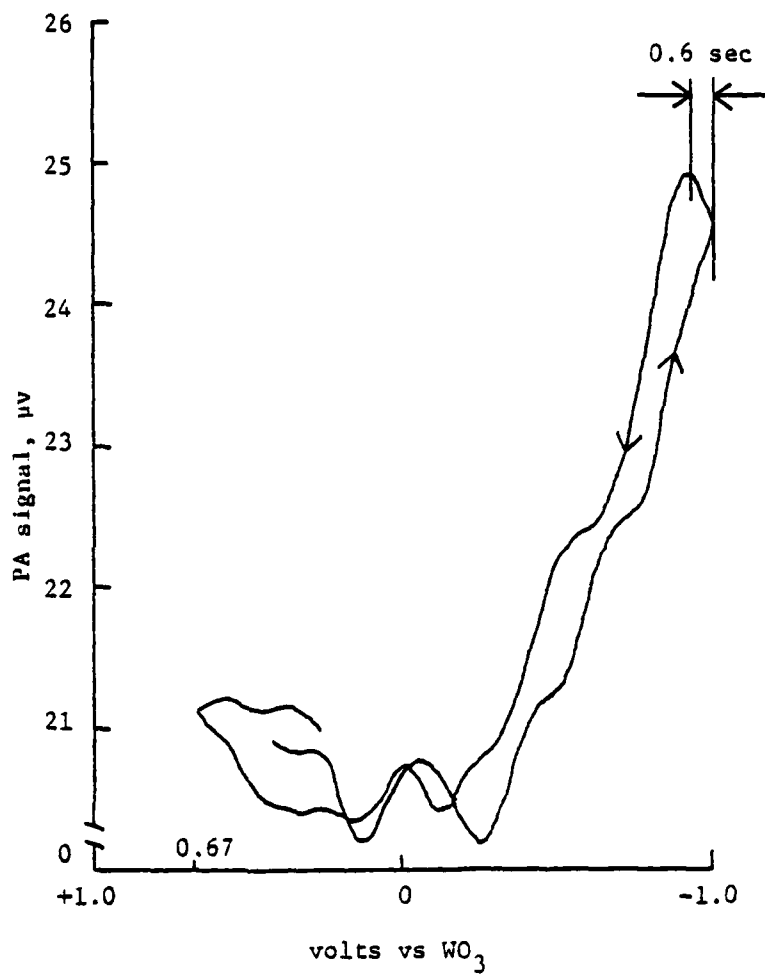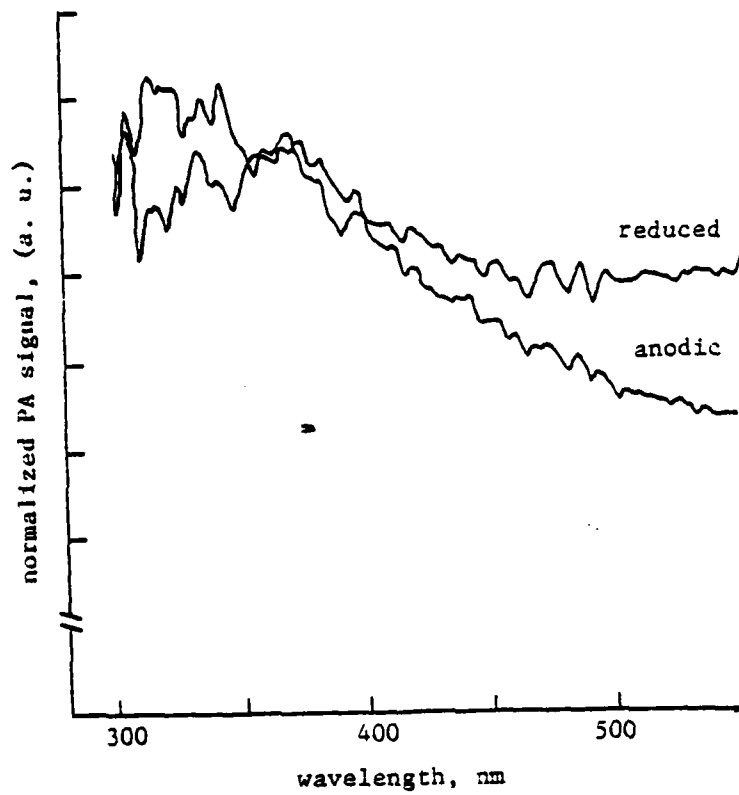Figure 24.   Normalized PA spectra of WO_3 anodic and
H_xWO_3 reduced films.

wavelength, nm

of thin films deposited on quartz substrates. The
peak of this broad band reported by Deb to be around
900 nm was not observed because of solution absorption
of the light at longer wavelengths.

Once the presence of the thin film was confirmed,
the correlation of film thickness to PA signal and a
minimum detectable thickness were determined. In a
preliminary experiment, WO_3 films were grown at four
thicknesses following the procedure used to make the
reference electrode. To a first approximation, based
upon a linear relation between applied potential
and film thickness [32] and assuming a maximum
thickness of 1.0 $\pm$ 0.2 µm at 75 vdc [ ] the estimated
film thicknesses are listed in Table II. The PA
spectrum showed no significant changes in character
or magnitude at any of these thicknesses.

Films were grown at a slower rate by cycling
at 100 mv/sec between 1.0 v and -0.67 v versus WO_3/W.
The film thickness at the end of the experiment was
determined by measuring cathodic coulombs (Q_c) as a
function of potential in the reduction to $H_x WO_3$ and
using

$$\lambda = \frac{(Q_c)\,(\text{molecular weight})}{X \cdot F \cdot d \cdot A}$$

where λ is the thickness in centimeters, F is Faraday's

TABLE II: APPROXIMATE WO_3 FILM THICKNESSES

| VOLTS DC	THICKNESS Å
10	1.3×10^3
21.5	2.9×10^3
47.5	6.3×10^3
65	8.7×10^3

constant, d is the density of anodic WO_3 (6.5 g/cm^3)
and A is the electrode area (cm^2). The fraction of WO_3
reduced, x, in an anodically grown film was determined
to be a function of potential by Reichman [31]. From
Equation (9) and Reichman's data, the WO_3 film thick-
ness at the end of the experiment was calculated to
be 730 $\pm$ 100 Å. Film thickness during the experiment,
calculated from coulometric measurements of the WO_3
reduction made at each thickness and based upon the
final thickness of 730 Å were 130, 210, 265, 390 and
560 Å.

PA spectra of WO_3 (bleached) representing
three of the six thicknesses observed are reproduced
in Figure 25. The signal magnitudes initially increased
with increasing WO_3 thickness, apparently without
losing the tungsten electrode spectral character.
At thicknesses greater than about 300 Å however, the
band edge of WO_3 became evident.

From the information obtained in these two
experiments, the WO_3 absorption coefficient for a
given energy was estimated. From the first experiment,
no change in the PA spectra signal magnitude indicates
the effective μ_s for the film-electrode system at
30 Hz chopping frequency was greater than μ_β and
greater than the thickness of the film-electrode

Figure 25.   Normalized PA spectra of WO_3 anodic films
at three thicknesses.
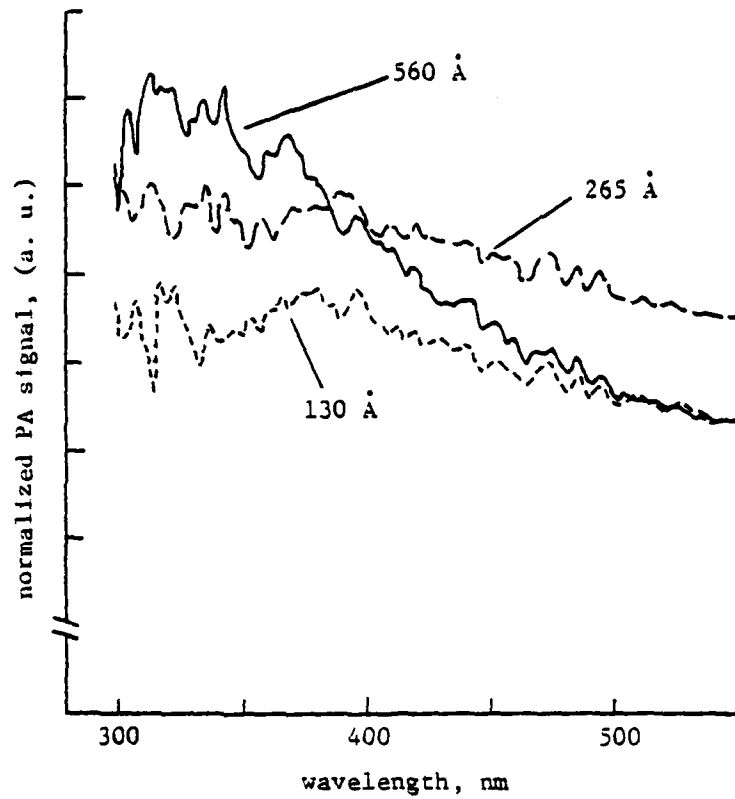
sample. Thus energy absorbed at the film surface was maximally transmitted through both the film and the electrode and the PA signal was independent of film thickness.

In the second experiment, the much thinner films were on the order of μ_β for WO_3 in band edge region, and exhibited a PA signal dependence on thickness. Figure 26, a plot of PA signal versus film thickness, illustrates that dependence. With 350 nm light, the PA signal increased rapidly until the film thickness was approximately equal to μ_β, when it became independent of thickness. Based upon a thickness of 225 ± 31 Å, where this transition takes place, the absorption coefficient for WO_3 at 350 nm was calculated as $4.4 \pm 0.6 \times 10^5$ cm^{-1}. The value reported by Deb, for an amorphous film was 5×10^4 cm^{-1}.

The increased PA signal without the development of the WO_3 spectral character (Figure 25) observed at thicknesses less than 300 Å can be attributed to absorption at the backing electrode.

If the thickness of the film is less than μ_β as predicted, it can be assumed that the tungsten electrode still absorbs a portion of the incident light energy and until the film is thick compared to μ_β, the PA spectrum will be some combination of the WO_3

Figure 26. PA signal dependence on WO_3 anodic film thickness. Error bars based on noise levels.
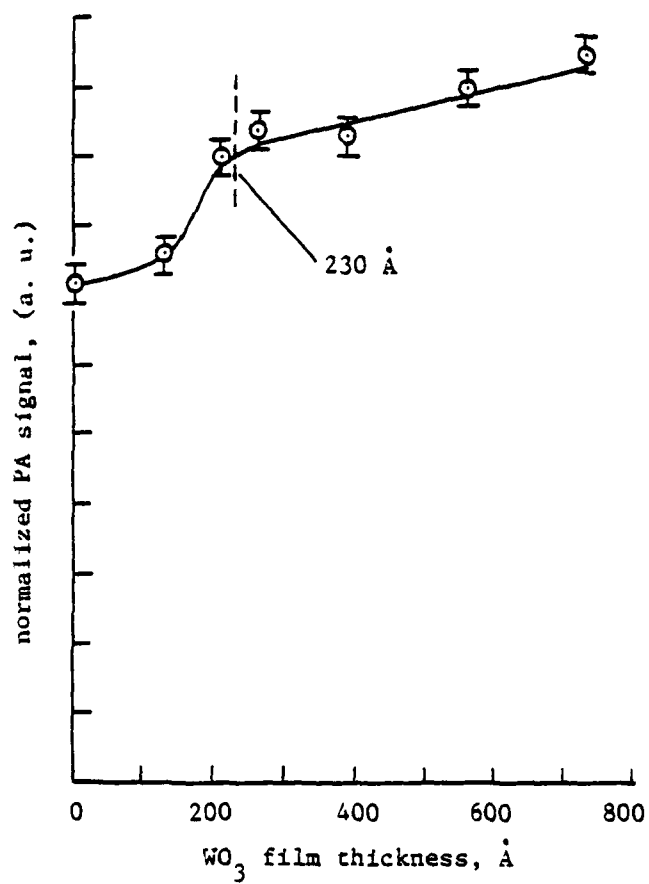
and tungsten spectra.

Chapter IV. PA Characterization of Titanium Dioxide

Semiconductor Powders and Crystals

Interest in the titanium dioxide (TiO_2)
semiconductor stems from its use in heterogeneous
photocatalysis, in which light energy absorbed by the
semiconductor is used to overcome the energy of activa-
tion of a chemical reaction. The process is based on
the production of holes and electrons by promotion of
electrons from a valence band to a conduction band.
Heterogeneous photocatalysis has been used in the
photo-decomposition of water [33], and hydrogen perox-
ide [34] and several other reactions [35].

The photoabsorption of TiO_2 is enhanced with
its reduction, where oxygen vacancies create defects
in the lattice structure and increase the number of
available donor electrons. This results in an increase
in the absorption coefficient of the semiconductor.
In this study TiO_2 powders and crystals were character-
ized with PA spectroscopy as to structure (rutile or
anatase) and to the degree of reduction.

Anatase or rutile

Anatase powder (Matheson Coleman and Bell, reagent
grade) sieved to particle sizes between 125-250 μm was
the starting material for all powders in these experi-
ments. To obtain rutile powders, an anatase sample

was heated in nitrogen at 820-850°C for more than 100 hours. PA spectra (obtained in the aluminum cell) identified the converstion by a red shift of the band gap energy by approximately 2.0 eV, Figure 27. Numerous authors have reported this shift observed with diffuse reflectance spectroscopy [36]. X-ray diffraction confirms the conversion from anatase to rutile, Figure 28.

Reduction of powders

The reduction of rutile TiO_2 powder to TiO_{2-x} is known to improve its electrical conductivity and is generally associated to a color change from off-white to gray and finally blue-black powders. The reduction of TiO_2 rutile powders was investigated with diffuse reflectance spectrscopy by Vratny [28] for x between 0.003 and 0.0109. Vratny reported the rutile powders became gray with increasing x, where x was determined by measuring with a Toepler pump-manometer the residual hydrogen after heat treatment with a known amount of hydrogen. For reduction in vacuum, x was determined by heating in the presence of finely divided nickel and then analyzing the nickel for oxygen content.

In this study, anatase and rutile powders were heated in vacuum and hydrogen respectively. Five samples of anatase powders were treated at 400°C for 0.5, 2, 5, 20 and 44 hours. At this temperature, there

Figure 27.   Normalized PA spectra of TiO_2 powder
(125-250 μm) converted from anatase to
rutile crystal structure. a) untreated
anatase, b) anatase/rutile mixture by
heating anatase in nitrogen at 840°C for
5 hours, c) complete conversion to rutile
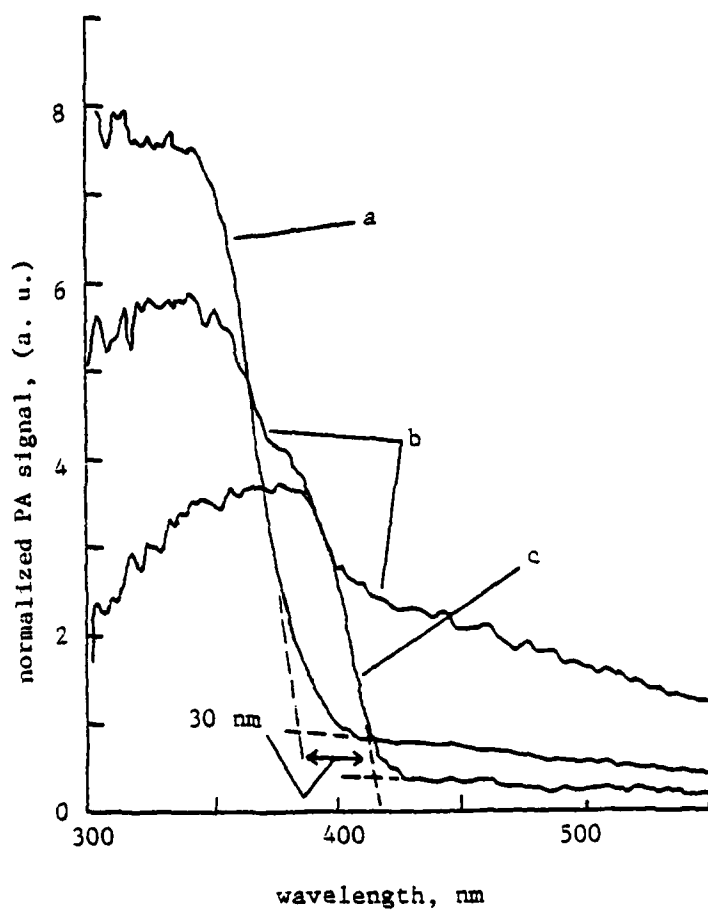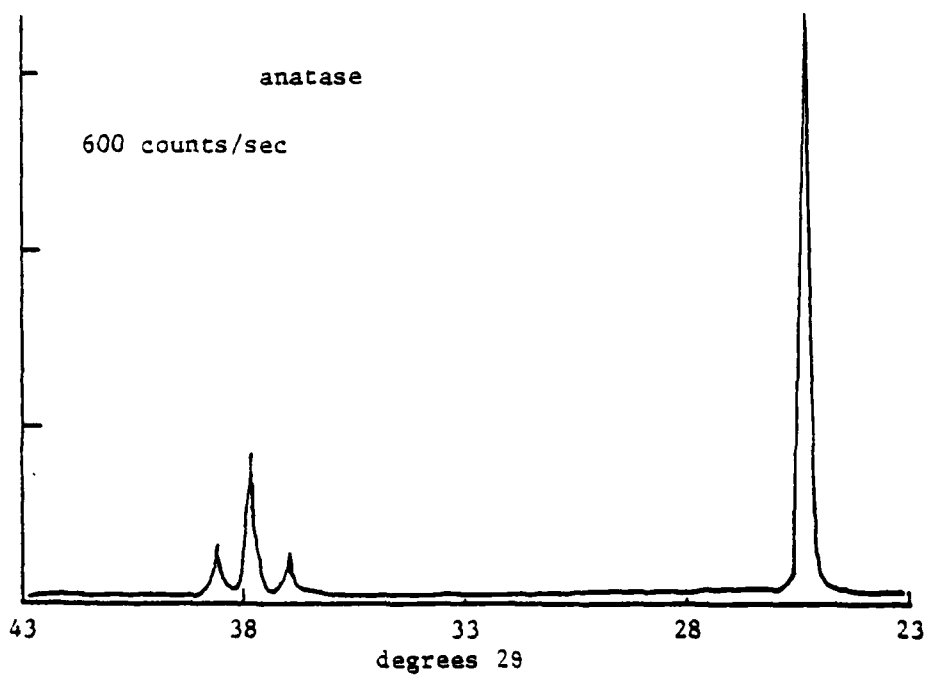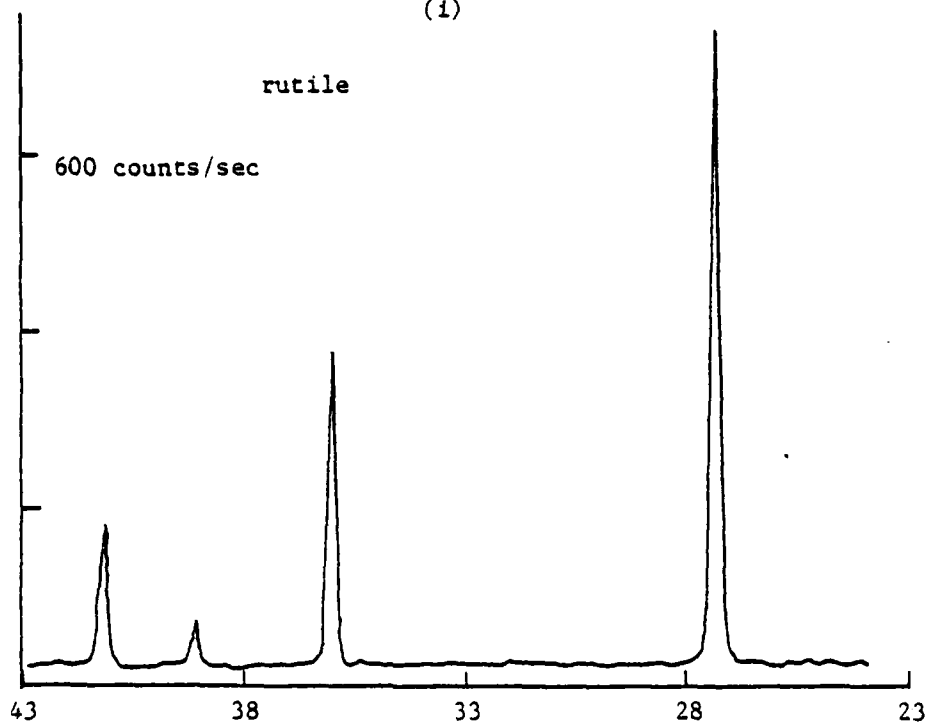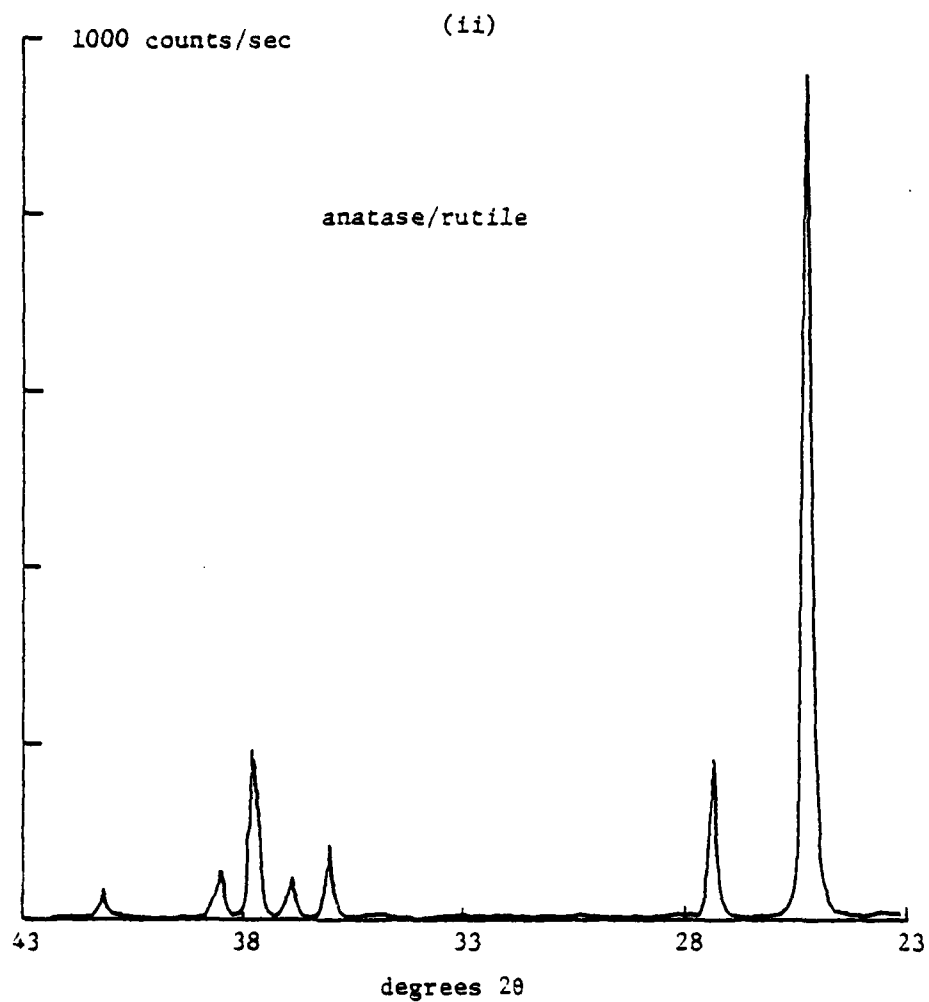by heating for 100 hours.

Figure 28. (i) X-ray diffraction of anatase (untreated) and rutile (heat for 100 hours in nitrogen at 840°C) powders.

(ii) X-ray diffraction of anatase/rutile mixture, by heating anatase in nitrogen at 840°C for 5 hours.

(i)

(ii)

1000 counts/sec

anatase/rutile

degrees 2θ

was no conversion to rutile as confirmed with both PA spectroscopy and x-ray diffraction. Color changes were gradual and only from white to biege. The PA spectrum of these samples and untreated anatase are shown in Figure 29. The PA signal at 350 nm and 500 nm is plotted as a function of heating time in Figure 30.

Heating caused some particles to agglomerate as observed under a microscope. Because the PA signal is proportional to the surface area of the sample, powders were re-sieved after heating to insure uniform particle size. However, it was also observed that the morphology of the powders changed upon heating. The untreated anatase powder, a rough surfaced particle, formed into a smoother surfaced sphere upon heating for even short durations. The subsequent reduction in surface area would result in a reduction of the PA signal magnitude.

The rutile powder samples were heated at 575°C for 2, 10, 20, 38, 60, 90 and 158 minutes and at 400°C for 2, 5, 15 and 60 minutes each. Sample colors varied from the untreated off-white rutile powder to darkening shades of gray. Again samples were sieved after heating. The PA spectra are shown in Figures 31 and 32, and the signals at 375 and 500 nm are plotted vs heating time in Figure 33.

Figure 29. Normalized PA spectra of anatase powders

treated in vacuum at 400°C for a) 0,

b) 0.5, c) 2, d) 5, e) 20, and f) 44 hours.

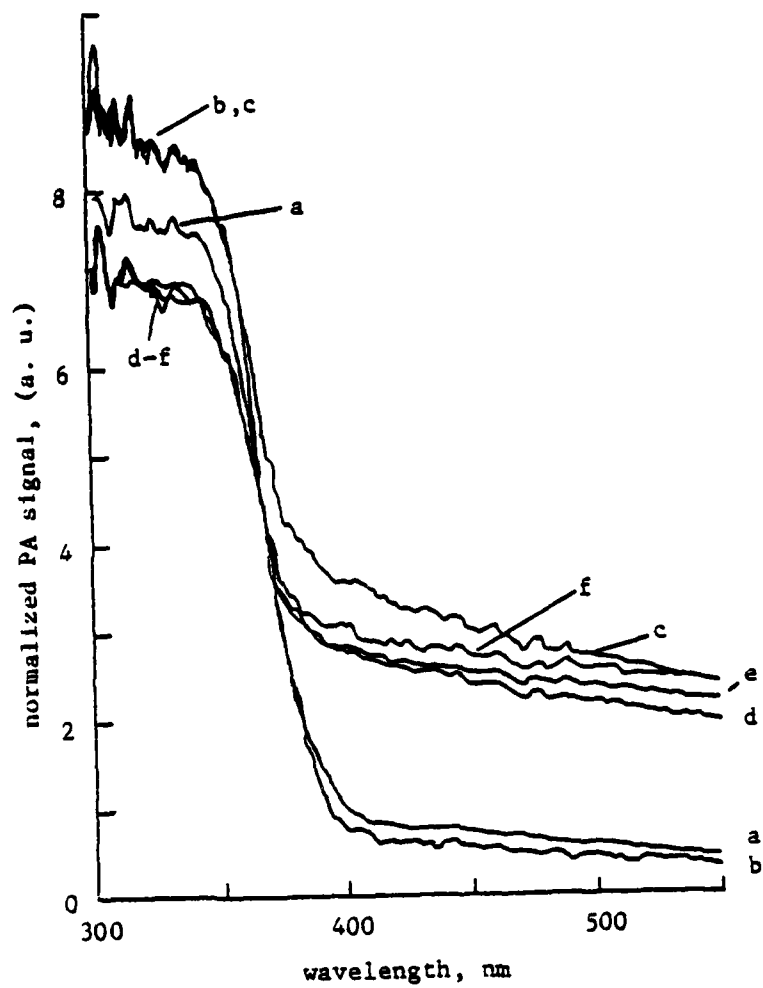normalized PA signal, (a. u.)

wavelength, nm

Figure 30. Normalized PA signal versus heating time for anatase powders treated in vacuum at 400°C.
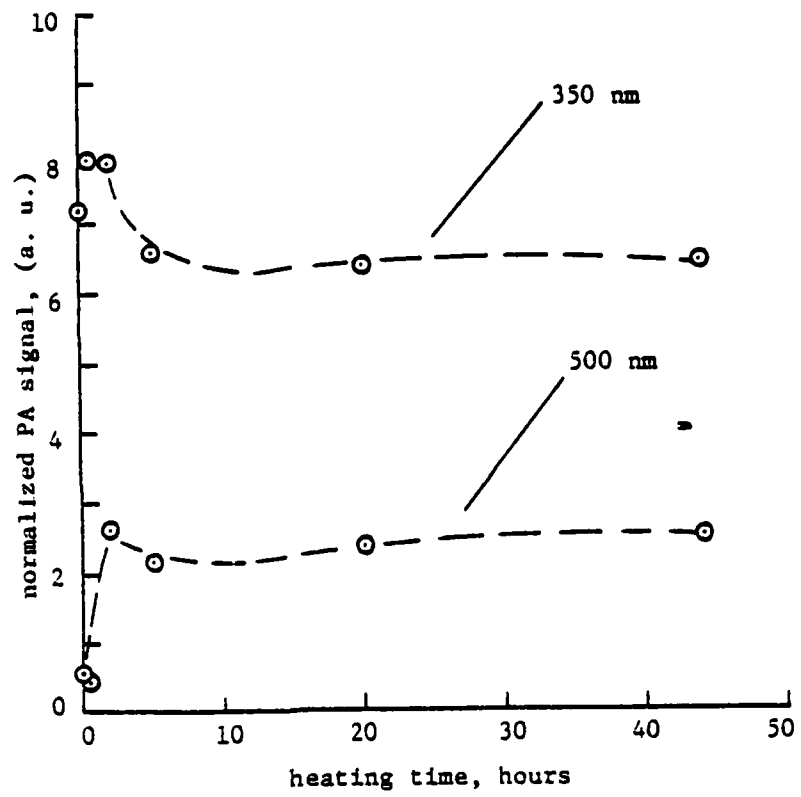
Figure 31.   Normalized PA spectra of rutile powders
treated in hydrogen at 400°C for a) 0,
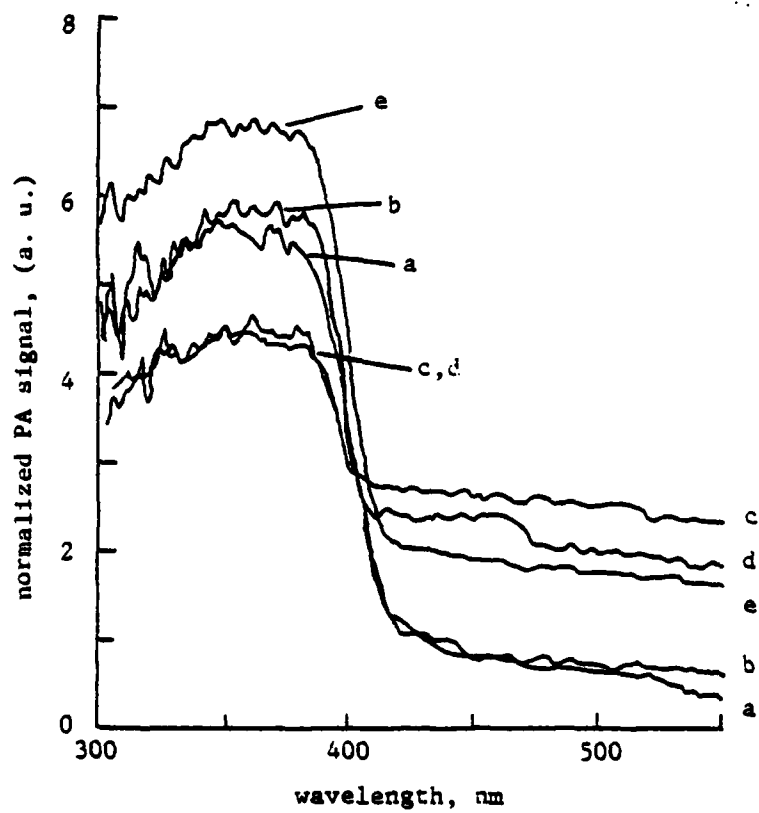b) 2, c) 5, d) 15, and e) 60 minutes.

98

Figure 32. Normalized PA spectra of rutile powders

treated in hydrogen at 575°C for a) 0,

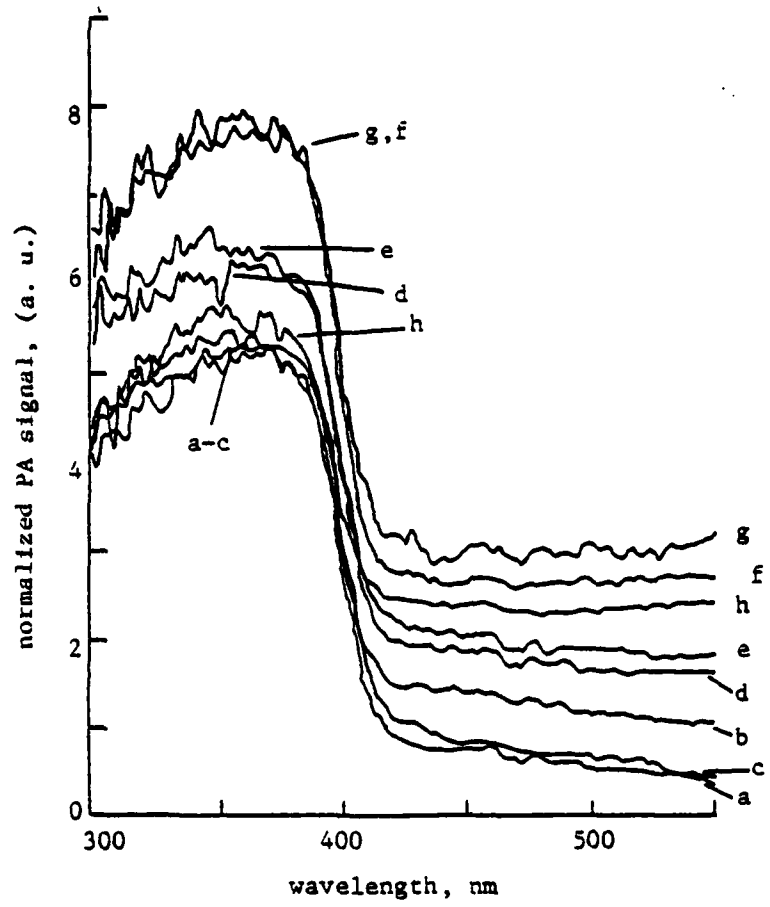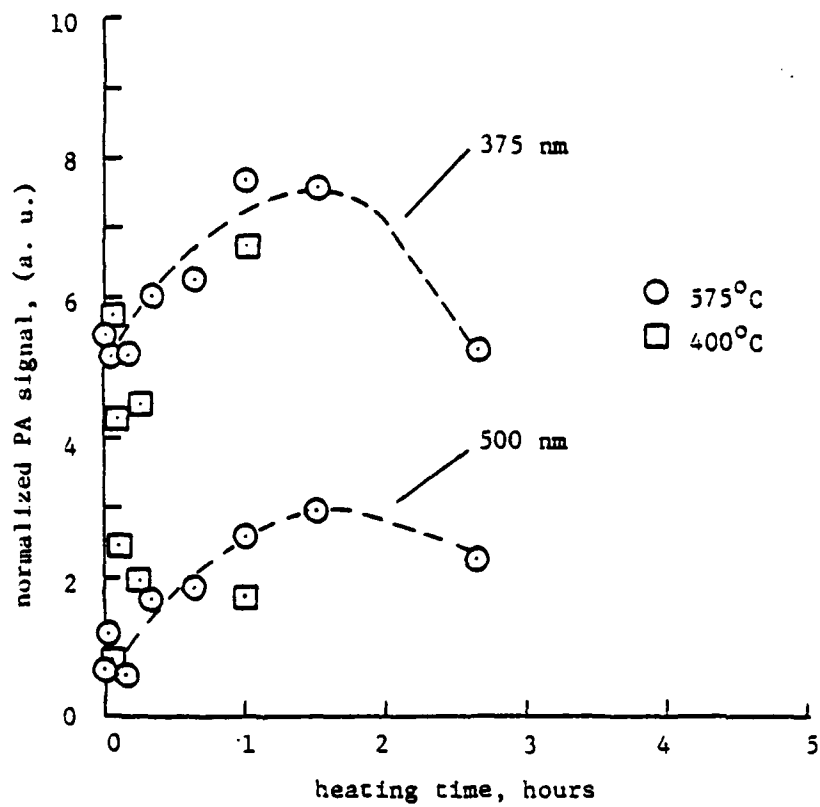b) 2, c) 10, d) 20, e) 38, f) 60, g) 90,

and h) 158 minutes.

Figure 33. Normalized PA signal versus heating time
for rutile powders treated in hydrogen
at 400°C and 575°C.

Reduction of rutile crystals

Rutile crystals obtained from fragments of single crystals were ground to particles less than 250 μm in diameter. The crystals, some of which were reduced to various degrees, were first treated under an oxygen flow at 700°C for 24 hours. This treatment returned the crystals to a milky white color and presumably TiO_2, unreduced. This one sample of crystals was treated a total of 310 minutes under hydrogen flow at 575°C. The sample was removed from the oven at 2, 12, 32, 70, 130 and 220 minutes and cooled under hydrogen. A PA spectra was obtained before resumption of heating. The color changes was from the initial milky white to blue-black crystals which did not show a color change after 60 minutes.

The PA spectra of the crystals corresponding to the seven heating times are shown in Figure 34. Figure 35 is a plot of PA signal at 375 and 500 nm versus the heating time.

Summary of PA data for reduced TiO_2

The dependence of the PA signal on the duration of the heating in the reduction TiO_2 anatase powders and rutile powders and crystals was shown in Figures 30, 33 and 35 for signals taken from the spectra at 500 nm, before the band gap, and at 375 nm (350 nm for

Figure 34. Normalized PA spectra of rutile crystals
treated in hydrogen at 575°C for a) 0,
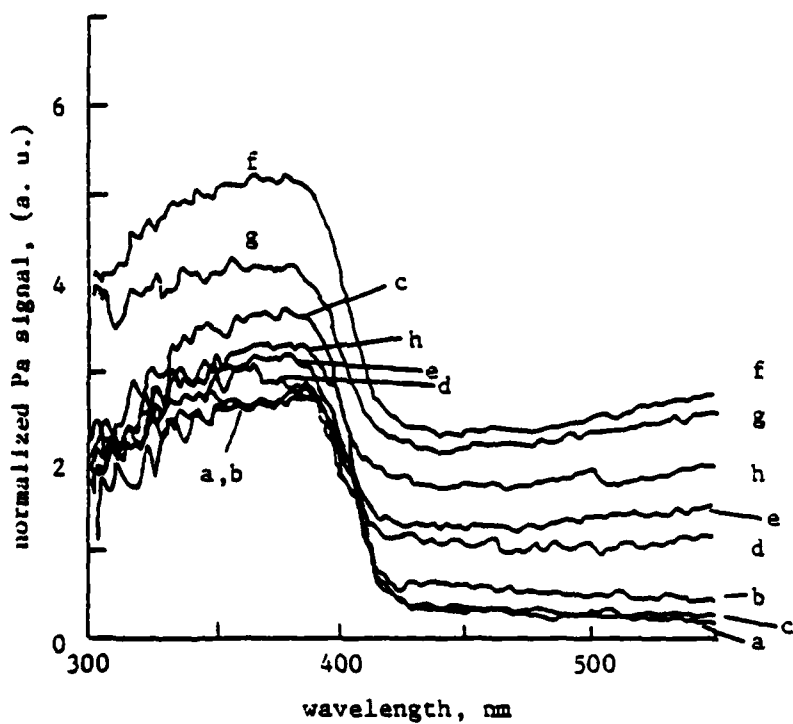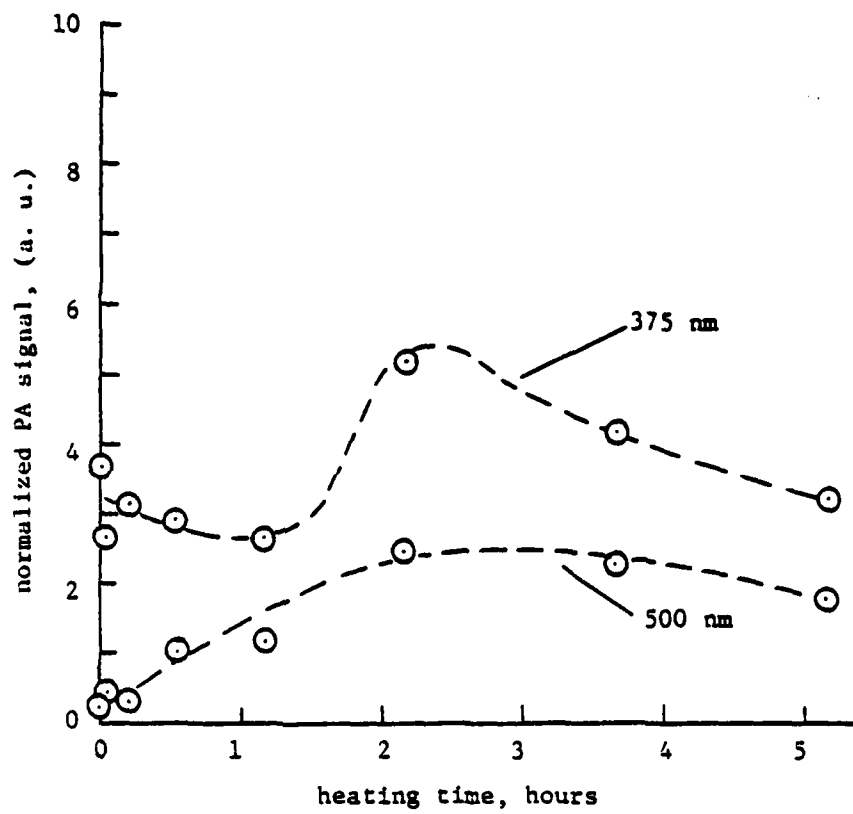b) 2, c) 12, d) 32, e) 70, f)130, g) 220
and h) 310 minutes.

wavelength, nm

Figure 35.   Normalized PA signal versus heating time
             for rutile crystals treated in hydrogen
             at 575°C.

normalized PA signal, (a. u.)

heating time, hours

anatase only) after the band gap. The PA signals for samples treated less than one hour are inconsistent, although the trend appears to be an increase in overall signal magnitude with increased duration of heating. With all samples, the PA signal peaks at 1-2 hours which is associated visually with the maximum color change. The PA signal changes observed in these samples are probably a result of the combined changes in the optical and thermal parameters of TiO_2 with heating.

TiO_2 single crystal

A TiO_2 rutile single crystal was cut to fit and fill the sample holder in the aluminum cell. A normalized spectrum is shown in Figure 36a along with the normalized spectra of a TiO_2 rutile powder (Figure 36b). The relative signal differences demonstrate the surface area effect on the PA signal. The PA signal at wavelengths greater than 420 nm results from the transmission of light through the single crystal and the subsequent absorption by the backing material. This is exaggerated in Figure 36c when black was used as the backing material. The dip in the normalized PA spectrum exists because the filtering of the light from the backing occurs faster than the PA response to the TiO_2 at the band gap.

Figure 36. Normalized PA spectra of rutile TiO_2.
a) powder (125-250 μm), b) single crystal
and c) single crystal with black backing
demonstrating transmission of low energy
light.

normalized PA signal, (a. u.) vs wavelength, nm
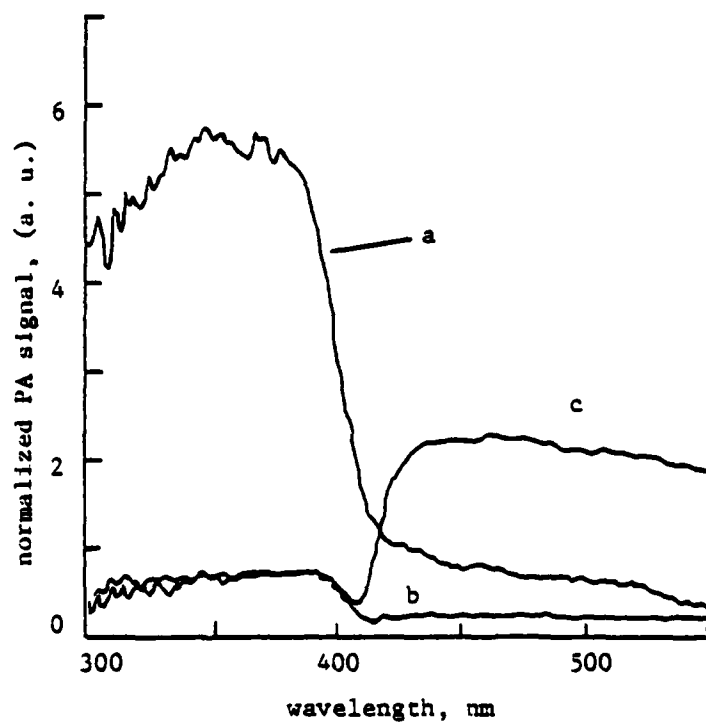
Chapter V. Summary

This work demonstrates the range of applications for the photoacoustic effect in absorption spectroscopy. The advantage of studying optical absorption by measuring the thermal energy produced from an electronic relaxation without scattered or reflected light interferences permitted the investigations of solid opaque materials and thin films on opaque electrodes. Previously absorption studies of this sort were carried out using transmission spectroscopy of very dilute solutions, or with thin films on transparent substrates. The complication involved in the PA techniques stem from the intertwining of absorption and thermal effects. Difficulties of this sort were observed in the saturation of the PA signal with the highly colored dyes rose bengal and p-nitroaniline, and in the PA spectra of the series of reduced TiO_2 powders and crystals.

PA techniques, coupled with electrochemical systems, produced both absorption spectra and a possible means of determining thermal and optical parameters of the materials involved. The fast coloration/bleaching process of the WO_3/H_xWO_3 system compared to the slower, thermally dependent PA responses could provide thermal diffusion data for both thin films and their backing electrodes by measurement of the

time delay of the PA signal relative to the time of coloration. It was also shown that from the changes in the PA response to different thickness of films (WO_3), absorption coefficients of that film could be determined. Techniques such as piezoelectric detection [37] of the thermal energy at the back of an electrode generated from photoabsorption of a thin film have produced similar results with much higher signal magnitudes.

The TiO_2 characterization study has left several questions unanswered. Although trends show the PA signal to increase upon the reduction of rutile and anatase samples, it is not confirmed that it is entirely due to the optical absorption. The complications of particle sizes and surface area effects and the possibility of changes in the thermal parameters accompanying the reduction have not been resolved. An experiment with a single rutile crystal treated similarly to the treatment of the powders and crystals reported here could eliminate the particle size and surface area effects, and would allow optical transmission spectra to identify changes in absorption.

References

1. M. E. Delany, Sci. Prog., 47, 459 (1959).

2. C. F. Dewey, Jr., R. D. Kamm, and C. E. Hackett, Appl. Phys. Lett., 23, 633 (1973).

3. A. Rosencwaig, Opt. Commun., 7, 305 (1973).

4. A. Rosencwaig, Phys. Today, 23 (1975).

5. P.-E. Nordal and S. O. Kanstad, Opt. Commun., 22, 185 (1977).

6. J. A. Noonan and D. M. Munroe, Opt. Spectra, 28 (1979).

7. F. A. McDonald and G. C. Wetsel, Jr., J. Appl. Phys., 49, 2313 (1978).

8. "Optoacoustic Spectroscopy and Detection", edited by Y.-H. Pao, Academic Press, New York (1977).

9. A. Rosencwaig and A. Gersho, J. Appl. Phys., 47, 64 (1976).

10. A. Rosencwaig and A. Gersho, Science, 190, 556 (1975).

11. M. J. Adams and G. F. Kirkbright, Spectrosc. Lett., 9, 255 (1976).

12. M. H. Adams, A. A. King, and G. F. Kirkbright, Analyst, 101, 73 (1976).

13. M. J. Adams and G. F. Kirkbright, ibid, 102, 281 (1977).

14. M. J. Adams, B. C. Beadle, and G. F. Kirkbright, _ibid_, 102, 569 (1977).

15. M. J. Adams, B. C. Beadle, and G. F. Kirkbright, _Anal. Chem._, 50, 1371 (1978).

16. M. J. Adams, B. C. Beadle, and G. F. Kirkbright, _Appl. Spectrosc._, 32, 430 (1978).

17. R. C. Gray and A. J. Bard, _Anal. Chem._, 50, 1262 (1978).

18. A. Rosencwaig and S. Hall, _Anal. Chem._, 47, 548 (1975).

19. A. Rosencwaig, _Science_, 181, 657 (1973).

20. D. Cahen, _Appl. Phys. Lett._, 33, 810 (1978).

21. D. Fournier, A. C. Boccara, and J. Badoz, _Appl. Phys. Lett._, 32, 640 (1978).

22. H. F. Olson and F. Massa, "Applied Acoustics", P. Blakiston's Son and Co., Philadelphia (1934).

23. H. T. van Dam and J. J. Ponjee, _J. Electrochem. Soc._, 121, 1555 (1974).

24. R. Jasinski, _J. Electrochem. Soc._, 124, 637 (1977).

25. S. K. Deb, _Philos. Mag._, 27, 801 (1973).

26. R. S. Crandall, P. J. Wojtowicz and B. W. Faughnan, _Solid State Commun._, 18, 1409 (1976).

27. B. Reichman and A. J. Bard, _J. Electrochem. Soc._, 126, 583 (1979).

28. F. Vratny and F. Micale, <u>Trans. Faraday Soc.</u>, 59. 2739 (1963).

29. J. C. Touchstone and M. F. Dobbins, "Practice of Thin Layer Chromatography", John Wiley and Sons, New York (1978).

30. G. Brilmyer (private communication).

31. B. Reichman (private communication).

32. A. K. Vijh, "Electrochemistry of Metals and Semi-conductors", Marcel Dekker, New York, 138 (1973).

33. A. Fujishima and K. Honda, <u>Nature</u>, 238, 37 (1972).

34. A. H. Boonstra and A. H. A. Mutsaers, <u>J. Phys. Chem.</u>, 79, 1940 (1975).

35. S. N. Frank and A. J. Bard, <u>J. Am. Chem. Soc.</u>, 99, 303 (1977).

36. A. L. Companion and R. E. Wyatt., <u>J. Phys. Chem. Solids</u>, 24, 1025 (1963).

37. R. Malpas and A. J. Bard, <u>Anal. Chem.</u>, (submitted).

VITA

Robert Carl Ligday was born in St. Cloud, Minnesota, on August 25, 1952. He graduated from St. John's Preparatory High School, Collegeville, Minnesota in 1970. After four years at the United States Air Force Academy, Colorado, he was commissioned a Second Lieutenant in the United States Air Force. From 1974-1977 he was assigned to the School of Aerospace Medicine, Brooks Air Force Base, Texas as a research chemist. In August 1977 he entered the graduate school of the University of Texas at Austin under an Air Force Institute of Technology program.

Forwarding address: Box 3000
                        McClellan AFB, CA
                        95652

This thesis was typed by Diane R. Mumme.